

Beach groundwater response to ocean processes and rain on a mild-sloping barrier island Implications for sea turtle nest flooding

Christiaanse, Jakob C.; Antolínez, José A.A.; Marshall, Christopher D.; Figlus, Jens; Dellapenna, Timothy M.; Reniers, Ad J.H.M.

DOI

[10.1016/j.coastaleng.2025.104795](https://doi.org/10.1016/j.coastaleng.2025.104795)

Publication date

2025

Document Version

Final published version

Published in

Coastal Engineering

Citation (APA)

Christiaanse, J. C., Antolínez, J. A. A., Marshall, C. D., Figlus, J., Dellapenna, T. M., & Reniers, A. J. H. M. (2025). Beach groundwater response to ocean processes and rain on a mild-sloping barrier island: Implications for sea turtle nest flooding. *Coastal Engineering*, 201, Article 104795. <https://doi.org/10.1016/j.coastaleng.2025.104795>

Important note

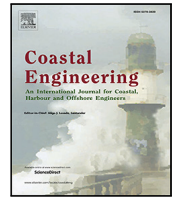
To cite this publication, please use the final published version (if applicable). Please check the document version above.

Copyright

Other than for strictly personal use, it is not permitted to download, forward or distribute the text or part of it, without the consent of the author(s) and/or copyright holder(s), unless the work is under an open content license such as Creative Commons.

Takedown policy

Please contact us and provide details if you believe this document breaches copyrights. We will remove access to the work immediately and investigate your claim.



Beach groundwater response to ocean processes and rain on a mild-sloping barrier island: Implications for sea turtle nest flooding

Jakob C. Christiaan^a ^{*}, José A.A. Antolínez^a, Christopher D. Marshall^{b,c}, Jens Figlus^d, Timothy M. Dellapenna^e, Ad J.H.M. Reniers^a

^a Department of Hydraulic Engineering, Delft University of Technology, Stevinweg 1, Delft, 2628 CN, Netherlands

^b Gulf Center for Sea Turtle Research, Department of Marine Biology, Texas A&M University at Galveston, 200 Seawolf Parkway, Galveston, 77554, TX, USA

^c Department of Ecology and Conservation Biology, Texas A&M University, 534 John Kimbrough Blvd, College Station, 77845, TX, USA

^d Department of Ocean Engineering, Texas A&M University, 200 Seawolf Parkway, Galveston, 77554, TX, USA

^e Department of Marine and Coastal Environmental Science, Texas A&M University at Galveston, 200 Seawolf Parkway, Galveston, 77554, TX, USA

ARTICLE INFO

Dataset link: <https://doi.org/10.4121/93256801-ed01-4627-9e49-8607967a0853>

Keywords:

Beach groundwater
Sandy beaches
Sea turtles
Nest flooding
Nature-based solutions
Spectral analysis
Field observations

ABSTRACT

Beach groundwater dynamics play a critical role in coastal ecosystem functions, particularly in low-lying beach habitats used for nesting by endangered species like sea turtles. Incubating nests are susceptible to prolonged inundation below the groundwater table (GWT), as flooding duration critically affects egg viability. Understanding how oceanic processes and rain drive GWT fluctuations in the nesting area is essential for evaluating nest relocation strategies and designing nature-based solutions that mitigate nest flooding. Here, we analyze how infragravity waves, tides, storm surge, and rainfall drive short-term fluctuations (hourly to weekly) in the beach GWT on Galveston Island, Texas—a dissipative, mild-sloping barrier island system along the northwestern Gulf of Mexico coast. Applying tailored spectral analyses to field observations collected in 2023, we show that surge and rainfall dominate short-term GWT response in the nesting area, while higher-frequency wave and tidal signals are increasingly damped landward. To facilitate this analysis, we classify observed water levels into *groundwater*, *mixed*, and *submerged* regimes based on estimated wave runup. A flooding threshold analysis reveals multiple, prolonged nest inundation events (exceeding 12 h) across the backshore, even for the shallowest nests. This strongly suggests that Galveston Island's beaches are currently unsuitable for turtle nesting, underscoring the need to continue the ongoing nest relocation program and further research nature-based solutions that enable sea turtle nesting (e.g., turtle-friendly nourishments).

1. Introduction

The increasing shift towards nature-based solutions in coastal engineering has led to a need for more research on how coastal processes and engineering interventions affect the local ecology, biodiversity, and ecosystem services (de Vriend et al., 2015; Nel et al., 2014). In this context, beach groundwater dynamics—the spatial and temporal variation of groundwater and moisture within the beach matrix—play a pivotal role in coastal ecosystem functions (Richardson et al., 2024), as they influence habitat health (Masterson et al., 2014), freshwater resources and salt intrusion (Bear et al., 1999; Holding et al., 2016), coastal flooding (Rotzoll and Fletcher, 2013; Delisle et al., 2023), and sediment transport dynamics (Bauer et al., 2009; Masselink et al., 2009). They are particularly important in low-lying habitats like barrier island systems (Holding et al., 2016; Housego et al., 2021; Masterson et al., 2014) and for endangered species like sea turtles, who depend on sandy

beaches for nesting. Yet, despite its significance, groundwater is often overlooked in the design and analysis of coastal interventions (Rotzoll and Fletcher, 2013).

Sea turtles—key species in many coastal ecosystems worldwide (e.g., Christianen et al., 2023; Meylan, 1988)—bury their eggs in beach sand, where they incubate for 6–8 weeks. Successful incubation requires a relatively narrow range of temperature and moisture conditions that facilitates the exchange of gases, water, and heat between the eggs and surrounding sand (Ackerman, 1997; Mortimer, 1990). Consequently, turtle nests are highly susceptible to sea- and freshwater inundation, which has been reported as a major threat to sea turtle populations (e.g., Gammon et al., 2023; Patrício et al., 2021; Van Houtan and Bass, 2007; Ware et al., 2021) and has motivated various management efforts, including nest relocation (Pintus et al., 2009). Although the species-specific tolerance of nests to inundation is not yet fully understood, recent studies suggest that both the duration

* Corresponding author.

E-mail address: j.c.christiaan@tudelft.nl (J.C. Christiaan).

and frequency of flooding events are critical factors affecting egg viability (Foley et al., 2006; Limpus et al., 2021; Pike et al., 2015). Flooding itself mainly occurs overland through wave runup, storm surges, high tides, rainfall, or a combination thereof. These driving processes can raise the groundwater table (GWT) in the nesting area of the beach. Given the significance of inundation duration, the response of the GWT to these processes plays a large role in determining the fate of individual nests (McGehee, 1990; Patino-Martinez et al., 2014). While studies that investigate the implications and drivers of nest inundation are increasing (e.g., Carpio Camargo et al., 2020; Caut et al., 2010; Gammon et al., 2023; Lyons et al., 2022), very few actively include the GWT in their analyses (Foley et al., 2006; Guard et al., 2008; Ware and Fuentes, 2018). Therefore, understanding what drives groundwater fluctuations in the nesting area of the beach is critical to evaluate the need for management practices like nest relocation and to design nature-based solutions that can help mitigate the flooding of turtle nests (Limpus et al., 2021; Ware and Fuentes, 2018).

Numerous studies have analyzed the influence of coastal hydrodynamics on beach groundwater. In general, both field studies (e.g., Nielsen, 1990; Raubenheimer et al., 1999; Turner et al., 1997) and laboratory experiments (e.g., Cartwright et al., 2004) have demonstrated that the beach matrix functions as a low-pass filter, resulting in the attenuation of oceanic fluctuations (e.g., tidal signal) in the GWT as they propagate inland, accompanied by increasing phase lag and asymmetry. Analytical and field observations have shown storm-driven pulses (due to surge and wave effects) in the GWT to propagate further and faster inland than tidal oscillations (Housego et al., 2021; Li et al., 2004). These oceanic forcings, along with rainfall, can drive considerable short-term variability (>1 m) in the beach GWT (Housego et al., 2021). Above the GWT lies the capillary fringe (CF), an additional saturated zone where negative pore pressures draw water upward from below (Gillham, 1984; Turner, 1993). On longer time-scales, the combination of tides and waves drives a super-elevation of the beach GWT, as it rises more quickly than it drops (Nielsen, 1989; Turner et al., 1997)—i.e., the mean GWT is above mean sea level. Furthermore, the GWT is expected to follow sea level rise (Bjerklie et al., 2012; Michael et al., 2013), which could compound short-term fluctuations, for example by increasing wave runup (Delisle et al., 2023).

Short-term variations in the GWT and the CF are influenced by a complex interplay of factors, including beach slope (Sous et al., 2013; Turner et al., 1997), sediment size and permeability (Gourlay, 1992; Raubenheimer et al., 1999; Turner et al., 1997), hydrological factors (Holding et al., 2016; Turner et al., 1997), and hydrodynamic forcing (Delisle et al., 2023; Turner et al., 1997). For instance, the relative super-elevation and CF width are expected to be higher in fine-grained, mild-sloping beach systems, which have lower permeability and therefore slower drainage (Turner and Nielsen, 1997). However, not all of these processes are fully understood and their interactions vary across different coastal environments, so it remains challenging to generalize findings between different environmental settings (Horn, 2006; Turner et al., 1997).

Here, we analyze how ocean processes and rainfall drive short-term (hourly to weekly) fluctuations in the beach GWT, specifically focusing on events that cause sea turtle nest inundation. We use data collected during an extensive field campaign in the fall of 2023 on Galveston Island, Texas, USA (Christiaanse et al., 2025)—a dissipative, mild-sloping barrier island beach system along the northwestern Gulf of Mexico coast. The observations enable us to assess the influence of infragravity waves, tides, storm surge, and rainfall on measured water levels between the shoreline and the dune toe. However, because the extent of the swash zone varied over time, the observed water levels did not always represent the pure beach GWT. To facilitate interpretation, we categorize the observed water levels into three regimes based on estimated wave runup: *groundwater*, *mixed*, and *submerged*. While we use the term GWT throughout this paper, our analysis explicitly focuses on ocean processes and rainfall acting directly on the beach system, and

does not include inland groundwater processes (e.g., aquifer recharge or regional groundwater flow). Our results (1) provide new observations on the interplay of coastal hydrodynamics and the beach GWT on mild-sloping beaches (to our knowledge, the first such observations in the Gulf of Mexico); (2) aid local coastal managers in evaluating nest relocation strategies; and (3) support research towards nature-based solutions that enable sea turtle nesting on Galveston Island (e.g., turtle-friendly beach nourishments).

2. Methods

2.1. Study area

Galveston Island is one of many low-lying barrier islands along the northwestern Gulf of Mexico coastline. It is located along the upper Texas coast, roughly 45 km southeast of Houston (Fig. 1a), and forms an important part of the Texas coastal protection system, as it shelters Galveston Bay from the Gulf of Mexico (USACE, 2021). Similar to other Texas barrier islands, Galveston Island began forming approximately 4500 years ago as submerged sandbars. These gradually evolved with an accumulation of fine sand deposits on top of older Pleistocene-era sediments (Garner, 1997). The island's surficial aquifer consists of a 10–15-m sand stratum, underlain by the confining *Beaumont Formation*—a Pleistocene unit primarily composed of clay with interbedded sand and silt (Capuano and Jones, 2022; Kreidler et al., 1977; Pettit and Winslow, 1957). The GWT is generally within a few feet of the surface (Garner, 1997). The surficial aquifer depth is comparable to those reported for other US barrier islands (e.g., the North Carolina Outer Banks; Housego et al., 2021). Following past studies, the regional aquifer structure is therefore approximated as homogeneous, despite small-scale heterogeneity (e.g., Housego et al., 2021; Rotzoll and Fletcher, 2013; Befus et al., 2020).

Galveston Island's beaches are mild-sloping and fine-grained ($D_{50} \approx 100$ – 160 μm ; see Christiaanse et al., 2025; Maglio et al., 2020; USACE, 2022, for full grain size distributions) and are backed by about 1–3 m-high dunes. In front of the city of Galveston — located on the northeastern part of the island — the beach is interrupted by groins every 300–500 m and backed by a 17 km-long concrete seawall, which essentially replaces the dune. Although situated in a mixed-diurnal micro-tidal setting (mean spring tidal range ± 0.8 m), local water levels show considerable variability, often deviating from the astronomical tide by a factor of two (NOAA, 2024). This variability is likely caused by a complex interplay of barotropic and baroclinic processes, such as atmospheric pressure variations and wind- and wave-induced setup (Huff et al., 2020). In addition, the region has experienced high sea level rise over the past century (around 6.5 mm/year since 1904) and is prone to hurricanes during the Atlantic hurricane season from June to November (Paine et al., 2021).

The Kemp's ridley (*Lepidochelys kempii*) is the main sea turtle species to nest on Galveston Island, with sporadic nesting by loggerhead sea turtles (*Caretta caretta*) (Valverde and Holzwart, 2017; Seney and Landry, 2008). The Kemp's ridley is the most critically endangered sea turtle in the World and is endemic to the western Gulf of Mexico, although more recently nesting is occurring in the northern Gulf of Mexico and southeast US coasts. The nesting season occurs from April to July for Kemp's, and from May to October for loggerheads (Marquez, 1994). Galveston Island is outside the historic Kemp's ridley nesting range (which lies further south in Mexico), but the species was introduced to Texas through a large-scale head-starting program over the past decades (Marquez et al., 2005; Shaver and Caillouet, 2015). As a result, the number of nesting females in Texas is steadily increasing. Moreover, Galveston Island's geographic position may enable it to become an important future climate refuge for the species. However, the continuous erosion and frequent inundation of Galveston's beaches combined with their low-elevation setting make it uncertain whether they can function as a suitable long-term nesting habitat for sea turtles.

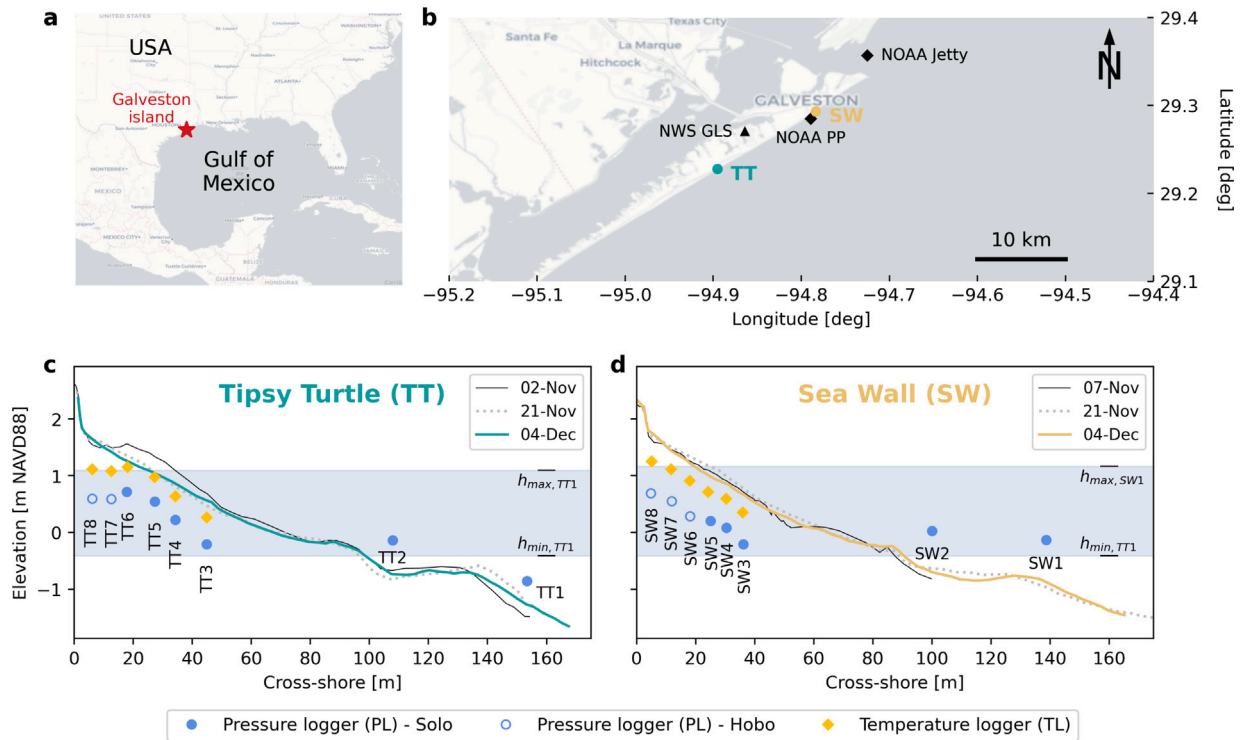


Fig. 1. (a) Location of the study area in North America. (b) Geographic overview of the study area. The two field sites are marked in their respective colors, and external observation stations (NOAA & NWS) in black. (c), (d) Cross-shore profiles and instrumentation at the two field sites.

Due to the critically endangered status of the Kemp’s ridley sea turtle, the current policy is to relocate all sea turtle nests in Texas to an incubation facility or corrals at Padre Island National Seashore, with a few exceptions (Shaver and Caillouet, 2015).

2.2. Field measurements and data

Measurements of groundwater, hydrodynamics, and sand characteristics were collected during the TURTLE field experiments on Galveston Island in the fall of 2023. Here, we give a summary of the part that is relevant for this study. For a detailed description of the complete field site, experimental setup, instrumentation, collected data, and technical validation, see Christiaanse et al. (2025). The local cross-shore coordinate systems and station numbers defined in Christiaanse et al. (2025) have been adopted here for consistency.

The data were collected at two field sites: *Topsy Turtle* (TT), located about 10 km southwest of Galveston (in front of the Topsy Turtle Sea Bar & Grill); and *Sea Wall* (SW), located in front of the sea wall between Galveston’s 18th and 19th Street (Fig. 1b). At TT the beach system is more natural with no recent nourishments, whereas nourishments have been carried out occasionally at the SW site. The main difference in the cross-shore profiles of the two locations was the initial presence of a berm on the backshore at TT, whereas the SW profile showed a fairly constant backshore slope (see black lines in Fig. 1c, d). This berm however eroded during storm conditions on 13/14 November, after which the two profiles were more similar.

For this study, we used the data from the two main deployments: 2 November to 4 December 2023 at TT (32 days) and 7 November to 4 December 2023 at SW (27 days). Both deployments had the same experimental setup, consisting of nine measurement stations along the cross-shore profile: At station 0, located about 1.5 km offshore, a directional wave buoy recorded the incoming wave conditions. At stations 1 and 2, submerged pressure loggers (PL) measured the incoming waves and water levels in the foreshore. Stations 3 to 8 were spread over the backshore, roughly between the high tide line and

the dune toe. At each of these six stations a PL measured the GWT inside a 1.5-m-deep slotted PVC well, and a buried temperature logger (TL) recorded the sand temperature at a typical turtle nesting depth (± 40 cm). Additionally, at station 8 (dune toe), a vertical array of six buried moisture, temperature, and electrical conductivity loggers (spaced at 10-cm depth intervals) was installed. Due to the berm at TT, the logger at station TT6 was deployed slightly higher than the ones at TT7 and TT8 (Fig. 1c), whereas the logger elevations at SW increased monotonically between SW3 and SW8.

Next to the field observations, we used astronomical tide predictions from NOAA station 8771510 (Pleasure Pier, PP) and observed water levels from station 8771341 (North Jetty; NOAA, 2024). We also used hourly precipitation totals from a weather station at Galveston Scholes Field Airport (GLS), accessible through the National Weather Service database (NWS, 2024). Finally, 30-year monthly precipitation statistics for Galveston were collected from the NCEI U.S. Climate Normals data base (NCEI, 2023).

2.3. Data processing

While most of the processing steps are described in detail in Christiaanse et al. (2025), we did a few additional processing steps here. The time series were recorded at varying sample rates, depending on the PL type (RBR Solo and Hobo U20L) that was used. At the upper well stations (TT7 and TT8 and SW6 to SW8) the Hobo loggers recorded at 1/15 Hz. At TT5, TT6, and SW5 we used 2-Hz RBR Solo’s and at all other stations 16-Hz RBR Solo’s. For the analyses presented in this study, we resampled the original time series to different time intervals depending on the analyzed process (Section 2.5).

Most time series contained short gaps caused by data offloads or other maintenance activities. These were generally in the order of minutes and were interpolated linearly to yield continuous time series. On 16 November all loggers were retrieved for 2–3 h for a data offload and maintenance check. This was done on the rising (falling) tide at TT (SW), so the resulting gaps did not include high or low water.

Therefore, they were linearly interpolated as well. However, some time series contained longer gaps that could not be interpolated. Specifically, there is no data at TT8 from 21 November 16:25 to 27 November 9:03, at SW5 from 13 November 13:15 to 14 November 10:30, and at SW8 on 13 November from 13:20 to 20:35 (all times in CST/UTC-6). In supplementary section S1, we explain the data gaps and how we handled them in this study in more detail.

2.4. Water level regimes and wave runup

The observed water levels at the backshore stations did not always represent the pure GWT, as some of the stations (particularly the lower ones) were regularly submerged, during high tide and surge events. When fully submerged, the observed water level represents the free surface elevation. Even when the beach at a given station was not fully submerged, water level observations may be affected by wave runup (wave setup + swash). Therefore, we classified the observed time series of the backshore stations (3–8) into three different water level regimes, based on the horizontal excursion of the mean water level at station 2 and the estimated 2%-exceedance value of the wave runup ($R_{2\%}$). These values were computed at 30-min intervals to classify the observed water levels as:

1. *Groundwater*: onshore of the $R_{2\%}$ position,
2. *Mixed*: between the $R_{2\%}$ position and the shoreline based on the water level at station 2,
3. *Submerged*: seaward of the shoreline.

We estimated the vertical elevation of $R_{2\%}$ based on [Stockdon et al. \(2006\)](#), who provide empirical formulations to compute $R_{2\%}$ from offshore wave conditions based on two components: wave setup and swash. They give a general formulation, which also includes the beach slope (β) and a formulation for very dissipative conditions, recommended for a surf similarity parameter $\zeta < 0.3$ (Iribarren number, after [Iribarren and Nogales, 1949](#)). Video-based observations of the wave runup at SW on 13 and 14 November 2023 showed that the dissipative formulation provided the most accurate $R_{2\%}$ estimate (RMSE = 0.08 m; [van der Grinten et al., 2025](#)), whereas the general formulation overestimated $R_{2\%}$, even for a mild beach slope ($\beta = 0.016$). The estimated wave runup must be added to a reference water level to compute the total elevation. Given that the observed water levels at stations 1 and 2 already include part of the wave setup, we used the dissipative $R_{2\%}$ formulation added to the observed water level at the NOAA Jetty station:

$$R_{2\%} = 0.043\sqrt{H_0 L_0} + h_{NOAA} \quad (1)$$

where H_0 and L_0 are the deep-water significant wave height and wave length, and h_{NOAA} is the 30-min observed water level at the NOAA Jetty. The offshore wave conditions were derived from wave conditions measured by the wave buoy at TT0, located at a water depth of about 8 m, approximately 1.5 km offshore of TT. We did not use the buoy at SW0 because it only recorded reliable data between 3 and 12 November 2023. However, the conditions measured at SW0 correlated very well with those at TT0 over this period ($r = 0.94$; [Christiaanse et al., 2025](#)). We used linear wave theory to convert the measured significant wave height, H_s , and peak period, T_p , to H_0 and L_0 ([Holthuijsen, 2007](#)). The deep-water wave length was computed as $L_0 = gT_p^2/2\pi$, while H_0 was derived from the linear shoaling coefficient ($H_0 = H_s/K_s$). The computation and formulae are explained in detail in the supplementary material (Section S2.1).

The wave buoy at TT0 was active between 3–26 November, after which it started drifting away ([Christiaanse et al., 2025](#)). Unfortunately, there was no alternative wave data available in the region, because the offshore NOAA wave buoy (ID 42035) was down during the entire deployment. However, the computed wave runup correlated well with $\sqrt{H_s L_0}$ at TT1 ($r = 0.88$) and SW1 ($r = 0.86$). We therefore used a linear

regression based on $\sqrt{H_s L_0}$ to derive the wave runup for the conditions outside the operational buoy window (mostly beyond 26 November). A detailed explanation of this interpolation and the final estimated $R_{2\%}$ are presented in the supplementary material (Section S2.2).

2.5. Spectral analysis

We used spectral analysis to quantify the influence of four driving processes on the observed groundwater fluctuations across the backshore (stations 3–8): infragravity (IG) waves, astronomical tide, rainfall, and storm surge. We excluded the water level on the bay side from this analysis, as it closely followed the sea level fluctuations and there was no significant change in the water level due to a residual sink or source (e.g., river inflow). We used the Fast Fourier Transform (FFT) to convert the observed time series from the time domain to the frequency domain. To ensure stationarity, we tailored the spectral analyses specifically to each driving process, explained in detail in the following sections.

2.5.1. Infragravity waves

To quantify the propagation of IG waves into the beach matrix we applied the FFT on the time-scale of sea states, assuming a stationarity window of 30 min. We used (resampled) 2-Hz time series where available (TT1 to TT6 and SW1 to SW5) and 1/15-Hz time series at the upper well stations (TT7 and TT8 and SW6 to SW8, see [Fig. 1c, d](#) for the instrument locations). The Nyquist frequency at the upper wells was therefore 1/30 Hz, giving a shortest resolvable wave period of 30 s. A common definition for the IG frequency band is from 1/250 to 1/25 Hz ([Bertin et al., 2018](#)), however that would have included waves with periods between 25 and 30 s, which could not be resolved from the 1/15-Hz time series. We therefore applied a bandwidth of 1/250 to 1/30 Hz in our analysis.

We used FFT to compute the power spectral density (PSD) over 30-min windows along each time series (except for the gaps). Following Welch's method, we divided each 30-min window into four blocks of 7.5 min ([Welch, 1967](#)). The final PSD was obtained by averaging the spectra computed over the four blocks. The choice of four blocks was based on a trade-off between reducing noise and retaining enough resolution to accurately resolve the longest periods in the considered IG bandwidth (250 s). We then used the n th-order spectral moment (m_n) of the PSD to compute the significant IG wave height ($H_{m0,IG}$) and mean IG wave period ($T_{m-10,IG}$; [Hofland et al., 2017](#); [Holthuijsen, 2007](#)):

$$m_n = \int_{1/250}^{1/30} f^n PSD(f) df, \quad (2)$$

$$H_{m0,IG} = 4\sqrt{m_0}, \quad (3)$$

$$T_{m-10,IG} = \frac{m_{-1}}{m_0} \quad (4)$$

2.5.2. Tide

Given that the astronomical tide is characterized by a sum of multiple constant harmonics, it is inherently stationary. In principle, spectral analysis through FFT is therefore well suited to analyze the propagation of the tide into the GWT. However, FFT does not directly provide information about the phase lag between the two time series, which is needed to understand how the ocean tidal signal is delayed in the GWT.

To analyze the propagation and relative phase shift of the tide, we computed the cross-spectral density (CSD), which is the Fourier Transform of the cross-correlation function between two time series. The magnitude and phase of the CSD represent the shared power and relative phase shift between the two signals at each frequency band, respectively. Combined with the PSDs of the individual signals, the CSD was used to compute the *coherence*, which quantifies the consistency of the relationship between the signals at each frequency band from 0 (no

coherence) to 1 (perfect coherence). Robust estimation of the CSD and coherence generally requires averaging over blocks to reduce noise and spectral leakage, as in Welch (1967). However, given our time series were relatively short compared to the dominant diurnal tidal periods, this would have led to poor frequency resolution.

We therefore used the multitaper method (MTM) introduced by Thomson (1982), a statistically robust alternative that enables spectral estimation over the entire time series using several orthogonal data windows (tapers). MTM is widely used in neuroscience but has also successfully been applied in hydrology (e.g., Van Hoek et al., 2016) and ocean sciences (e.g., Anarde et al., 2020; Jeyaseelan and Balaji, 2015; Percival and Walden, 1993). In short, the original time series is tapered (= multiplied) by k members of the Slepian functions (Slepian, 1978), which are orthogonal and thus statistically independent. From the resulting tapered versions of the original time series, k statistically independent *eigenspectra* are computed through FFT. The final spectrum is obtained by the (weighted) average of the k eigenspectra. Compared to conventional spectral analysis, MTM reduces bias and spectral leakage (Babadi and Brown, 2014; Bronez, 1992; Percival and Walden, 1993). Moreover, it is possible to derive an internal estimate of the variance through *jackknifing* (Thomson, 2007).

To reduce high-frequency noise, we resampled the time series to 10-min intervals. We then used the *multi_taper_csd()* function from the *Nitime* python library (Nitime, 2019) to estimate the PSD at each station and the CSD between station 1 and every other station. We used a time half-bandwidth of $NW = 3$, yielding $k = 5$ tapers. The tapers were adaptively weighted and filtered for low bias using the *adaptive_weights* and *low_bias* options in *Nitime*. The phase difference was computed as the argument (angle) of the complex CSD estimate, resulting in a value between $-\pi$ and π (radians) at each frequency. A positive (negative) phase difference translated to a lag (lead) in the signal compared to station 1. Hereby, the phase wraps around the two limits $[-\pi, \pi]$, which represent a fully out-of-phase signal. The time lag/lead at each frequency (f) was computed by dividing the phase difference by $2\pi f$. The coherence, $C_{x,y}(f)$, between each pair of time series (x and y) was computed as:

$$C_{x,y}(f) = \frac{|CSD_{x,y}(f)|^2}{PSD_x(f) \cdot PSD_y(f)}, \quad (5)$$

where $CSD_{x,y}(f)$ is the cross-spectral density and $PSD_{x(y)}(f)$ is the power spectral density of x (y). We quantified an uncertainty estimate for the coherence and the phase difference using a *jackknifing* technique, as outlined in Thomson (2007). This involved creating k separate estimates using a “leave-one-out” approach—i.e., estimating the coherence and phase k times by excluding one of the k tapers every time. The internal variance of the coherence was then derived from the error between each separate estimate and the average estimate. For the circular phase, we used a simple uncertainty estimate based on the maximum and minimum of the $k-1$ jackknife estimates. For a detailed explanation of the coherence and phase uncertainty estimation, we refer to supplementary section S3.1.

We quantified the amplitude decay and phase lag of the tidal signal across the stations over two frequency bands based on the dominant diurnal and semi-diurnal constituents at Galveston Island. At NOAA’s Pleasure Pier Station (NOAA PP in Fig. 1b), the diurnal tide is dominated by the K_1 , O_1 , P_1 , and Q_1 coefficients, with a combined amplitude of ± 42 cm. The semi-diurnal tide is dominated by the M_2 , S_2 , and N_2 coefficients, with a combined amplitude of ± 21 cm. Based on the frequencies of these harmonics and the frequency resolution and width of the tidal spectral peaks in the computed PSDs, we defined:

- The diurnal frequency band between $1 \cdot 10^{-5}$ and $1.25 \cdot 10^{-5}$ Hz (22.2 to 27.8 h periods).
- The semi-diurnal frequency band between $2.12 \cdot 10^{-5}$ and $2.35 \cdot 10^{-5}$ Hz (11.8 to 13.1 h periods).

To quantify the tidal amplitudes at each station, we took the square root of the integrated PSD over the corresponding frequency band:

$$A_{t,i} = \sqrt{\int_{f_{low}}^{f_{hi}} PSD_i(f) df}, \quad (6)$$

where $A_{t,i}$ is the total diurnal or semi-diurnal amplitude at station i , $PSD_i(f)$ is the PSD at station i , and f_{low} and f_{hi} represent the limits of the frequency band. We then quantified the phase lag (in hours) of the (semi-)diurnal tide at each station relative to station 1. The phase lag was computed as the average of all CSD phase values within the respective frequency band, retaining only frequencies with coherence $C \geq 0.5$. This threshold ensured that the estimated phase lag was based on coherent frequency components only.

This analysis required full continuous time series without missing data. Therefore, we interpolated the data gaps at TT8, SW5, and SW8 (see Section 2.3) linearly, even though this may have introduced artifacts. The results were interpreted with this caveat in mind. At SW5 (± 21 h) and SW8 (± 7 h) the gaps were relatively short, so we do not expect the results to be affected significantly.

2.5.3. Surge and rainfall

The stationarity assumption does not hold for the surge component of the total water level. As the corresponding frequencies are not known a priori and may vary over time, isolating the meteorological surge signal from the rest of the time series was difficult. We applied a low-pass FFT filter to reconstruct the low-frequency signal at each station. We used the same 10-min resampled time series as for the tidal analysis and a cut-off period of 36 h ($\approx 7.7 \cdot 10^{-6}$ Hz) for the FFT filter, to prevent potential spectral leakage of the diurnal tide (± 25 -h period) from influencing the surge signal.

Next to the meteorological surge, the low-passed time series also included residual components, such as low-frequency tidal variations and the smoothed GWT response to rainfall. Based on the tidal predictions at NOAA PP, there are two relevant low-frequency tidal constituents that we could not isolate from the signal: solar semi-annual (SSA) and solar annual (SA) (NOAA, 2024). However, both have amplitudes below 10 cm, so on the time-scale of our observations (± 30 days), we assumed these to be negligible relative to the surge component. Moreover, the foreshore water levels should not be affected by rainfall. We therefore assumed the low-passed signal to be an acceptable proxy for the meteorological surge at stations 1 and 2. At the groundwater stations (3–8), however, the response to rainfall was significant in the low-passed signal. Due to the lack of local high-resolution rain data and the difficulty of separating the surge and rain responses in the groundwater, we decided to include the rainfall in this part of the analysis. It should be noted, however, that the actual response of the GWT to rainfall occurs on shorter timescales (minutes to hours). We discuss this further in Section 4.1.

We selected five separate events to analyze the groundwater response to the surge and rainfall from the low-passed signals (Table 1). We used hourly precipitation rates from the GLS weather station (NWS GLS in Fig. 1b) and two-hour averaged wind speed and direction data from the NOAA’s North Jetty station (NOAA Jetty in Fig. 1b), to determine whether each of the five events was influenced by surge, rain, or both. One event was rain-only, two events surge-only (one with a reverse surge), and two storm events with both surge and rain. For each event we analyzed the corresponding maxima (minimum for the reverse surge) in the low-passed signals across the station. The amplitude at each station was computed as the difference between the maximum and the preceding minimum (vice-versa for reverse surge) and the time lag was quantified relative to the maximum (minimum) at the most seaward station. Data gaps that could not be interpolated (see Section 2.3) were excluded from the analysis, meaning that TT8 was excluded from the reverse surge and surge, and SW5 and SW8 were excluded from storm 1.

Table 1
Overview of events considered in the low-pass FFT analysis of groundwater response to the meteorological surge and rainfall.

Event name	Date	Surge influence	Rain influence
Rain	9/10 Nov	No	Yes
Storm 1	13/14 Nov	Yes	Yes
Reverse surge	21/22 Nov	Yes (negative)	No
Surge	25/25 Nov	Yes	No
Storm 2	30 Nov/1 Dec	Yes	Yes

2.6. Nest flooding analysis

Kemp’s ridley turtles typically nest between the high tide line and the first dune, with most nests near the vegetation line in front of the first dune, and their nests are typically 30–40 cm deep (Culver et al., 2020; Marquez, 1994). That mainly corresponded to the area covered by the upper three stations (6–8) at each site. For each of these stations, we quantified the number and duration of nest inundation events. An inundation event was defined as the GWT exceeding the nest depth threshold and lasted until the GWT dropped below the threshold again.

We used a threshold of 30 cm below the sand surface at the start of the deployment, representing the shallowest nests.

Given the data used in this study was mostly gathered in November 2023, outside the nesting season, our results were not directly transferable to actual nests, which are in the sand from April to potentially late September. Therefore, we performed a statistical comparison of historical water levels and rainfall rates between the nesting season and November to assess if similar conditions could be expected. We used 23 years of historical hourly water levels at the North Jetty station (2001–2023) which we detrended using simple linear regression to account for sea level rise. For rainfall, we used 30-years monthly precipitation normals from the GLS weather station (1991–2020).

3. Results

3.1. Observed water levels

There was considerable variability in the observed water levels, both at the foreshore stations (1 and 2) as well as the backshore stations (3–8, Fig. 2). In the foreshore the mean water level was around 0.35 m + NAVD88 (North American Vertical Datum of 1988) and the total range was about 1.6 m (double the mean spring tidal range in the area

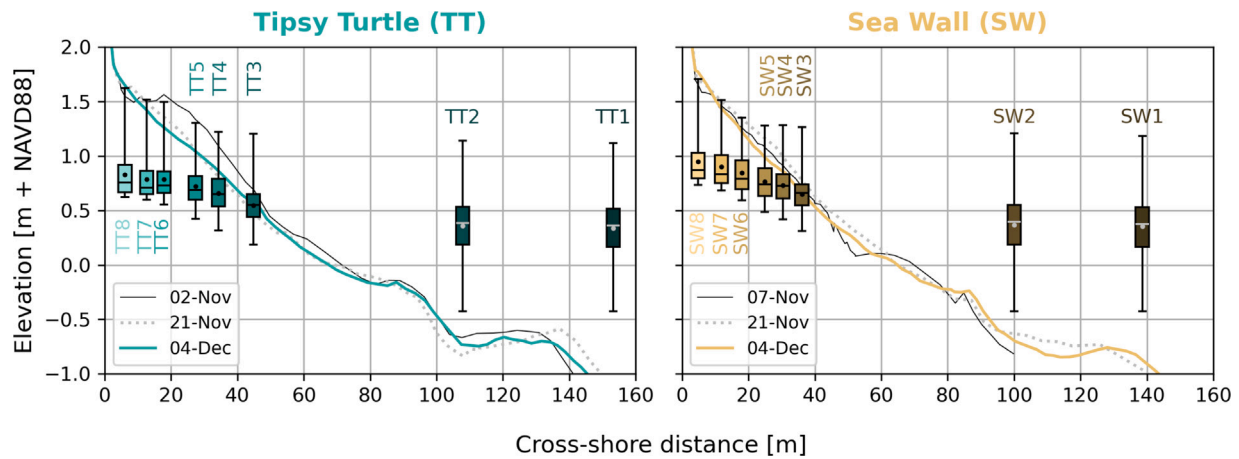


Fig. 2. Summary of observed (ground)water levels across the field stations. Boxes show the inter-quartile range, whiskers the entire observed range, bars the median, and dots the mean. The corresponding bed profiles are shown for reference.

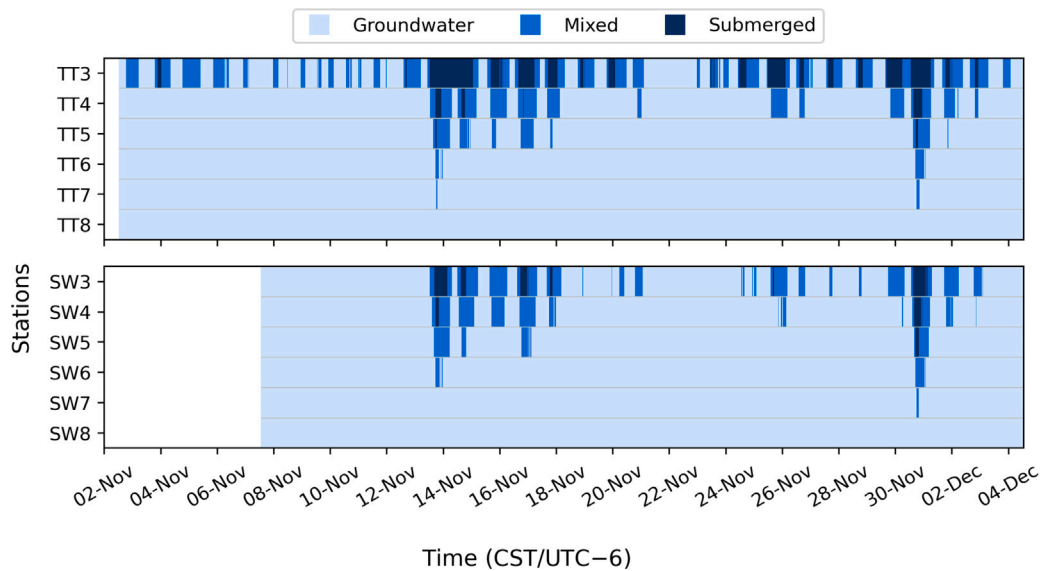


Fig. 3. Water level regimes (every 30 min) at the backshore stations of TT (upper panel) and SW (lower panel). The observed water levels are categorized into three regimes: groundwater (beach surface above $R_{2\%}$), mixed (beach surface between $R_{2\%}$ and water level at station 2), and submerged (beach surface below water level at station 2).

of ± 0.8 m). The mean water level at the backshore stations steadily increased towards the dune to 0.83 m (0.95 m) at TT8 (SW8), resulting in a super-elevation of about 0.5–0.6 m at the dune toe. The observed water levels also became increasingly positively skewed towards the dune. Notably, the lowest observed GWT at the six upper backshore stations (6–8) was above the mean water level in the foreshore. The total range varied but was in the region of 1 m at most backshore stations, roughly two-thirds of the water level range in the foreshore. Note that the time series at TT6, TT8, SW5, and SW8 contained some gaps which may have slightly influenced the results presented in Fig. 2 (see also Section 2.3).

Based on the water level regimes, the lowest groundwater stations (TT3/SW3) were submerged several times during high tides, particularly TT3 (Fig. 3). TT4, SW4, TT5, and SW5 were mainly submerged during the two storm events. All lower backshore stations (3–5) had significant periods of mixed water level regimes, when the station was between the $R_{2\%}$ and waterline. Particularly TT3, which had the

lowest elevation of all backshore stations, was in mixed or submerged conditions roughly 50% of the time. All other stations were in the groundwater regime at least 75% of the time. At stations 6–8 the observed time series mainly reflected groundwater conditions, with only short periods of the mixed regime during the storms at stations 6 and 7.

3.2. Drivers of GWT fluctuations

3.2.1. IG waves

Most of the IG wave energy was observed during the two storms on 13 and 30 November, when the significant IG wave height, $H_{m0,IG}$, reached up to 23 cm in the foreshore (Fig. 4). This storm IG energy generally increased at the lower backshore stations (3–5), with $H_{m0,IG}$ reaching 40+ cm. During these conditions, the water level at all three lower stations represented mixed or submerged conditions (not the GWT). The IG wave height within the inner surf and swash is a result

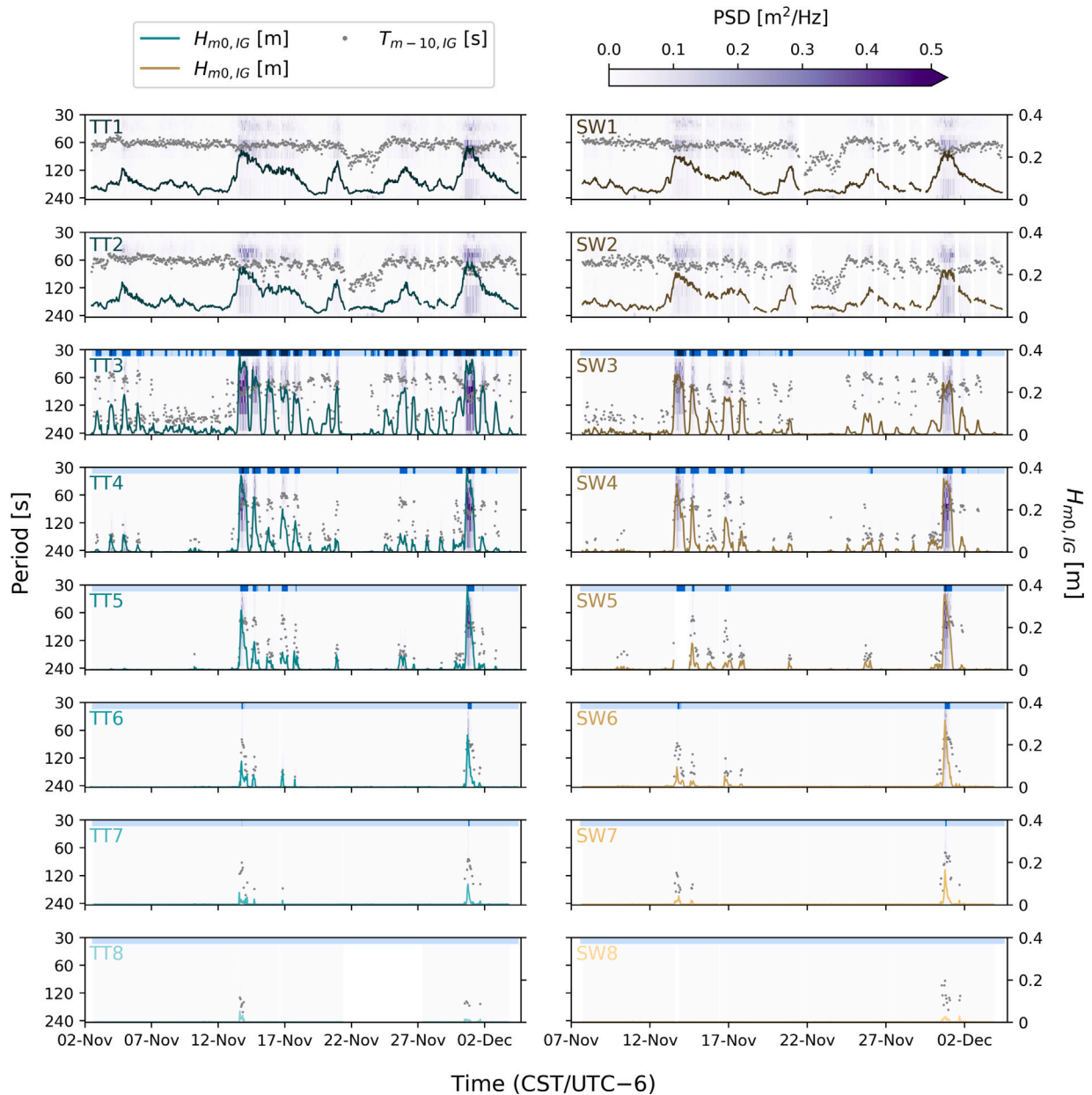


Fig. 4. Infragravity spectrograms at TT (left column) and SW (right column), from station 1 (top) to station 8 (bottom). The solid colored lines represent $H_{m0,IG}$, while the grey dots represent $T_{m-10,IG}$ (only plotted for $H_{m0,IG} > 1$ cm, to filter noise). Frequencies were converted to periods for visualization. The blue shaded bar at the top of the subplots of stations 3–8 shows the water level regime over time: groundwater (lightest), mixed (middle), submerged (darkest), see also Fig. 3.

of the balance between shoaling, dissipation by breaking, bed friction, reflections, and the non-linear transfer from the sea-swell to the IG waves leading up to it (Henderson and Bowen, 2002; Thomson et al., 2006). These processes are controlled by the beach slope, with shoaling generally stronger on milder slopes (Battjes et al., 2004; van Dongeren et al., 2007). Conservation of energy flux ($H^2 \sqrt{gh} = \text{constant}$) with water depths of $h \approx 2.5$ m (TT1), 2 m (TT2), and 0.5 m (TT3) during the storms would result in shoaled wave heights of about 1.05 (TT2) and 1.5 (TT3) times higher than at TT1. This is roughly consistent with the observations in Fig. 4, showing that the IG waves shoal before dissipating by breaking and friction.

IG energy at the backshore stations was also highly dependent on the tide, with $H_{m0,IG}$ dropping to zero during almost every low tide, suggesting that IG oscillations only have a strong influence in the swash zone. Consequently, at the upper groundwater stations (6–8), IG response was primarily limited to the two storm events, with minimal IG energy observed at the dune toe (station 8).

In the PSDs of TT1 and SW1, IG energy was mainly concentrated around three bands (see purple shaded PSDs in Fig. 4). The main band had periods of 60–70 s. A second, lower energy band was at 30–40-s periods, and a third band at longer periods (120–200 s), mainly visible during the storms. At TT2/SW2, the first two IG bands appeared to have

Table 2

Mean IG wave period $T_{m-10,IG}$ (s) across the three water level regimes and the stations at TT. Only periods with $H_{m0,IG} \geq 1$ cm were included, to filter out noise. The bimodal character $T_{m-10,IG}$ is clearly visible from the longer periods during groundwater conditions compared to mixed/submerged conditions.

	TT1	TT2	TT3	TT4	TT5	TT6	TT7	TT8
Submerged	66	68	73	81	83	–	–	–
Mixed	–	–	92	86	88	83	82	–
Groundwater	–	–	163	166	157	142	134	162

merged into a single band concentrated around 50–60-s periods. At the backshore stations, the IG periods showed a bimodal character, linked to the water level regimes (Table 2). During mixed and submerged conditions, $T_{m-10,IG}$ was similar to the period in the foreshore. During groundwater conditions, $T_{m-10,IG}$ was significantly larger, along with a smaller $H_{m0,IG}$. This pattern suggests that the shorter IG bands visible in the foreshore were damped out rapidly and only the longer-period band propagated into the GWT, consistent with earlier studies showing frequency-dependent attenuation (e.g., Nielsen, 1990; Turner et al., 1997).

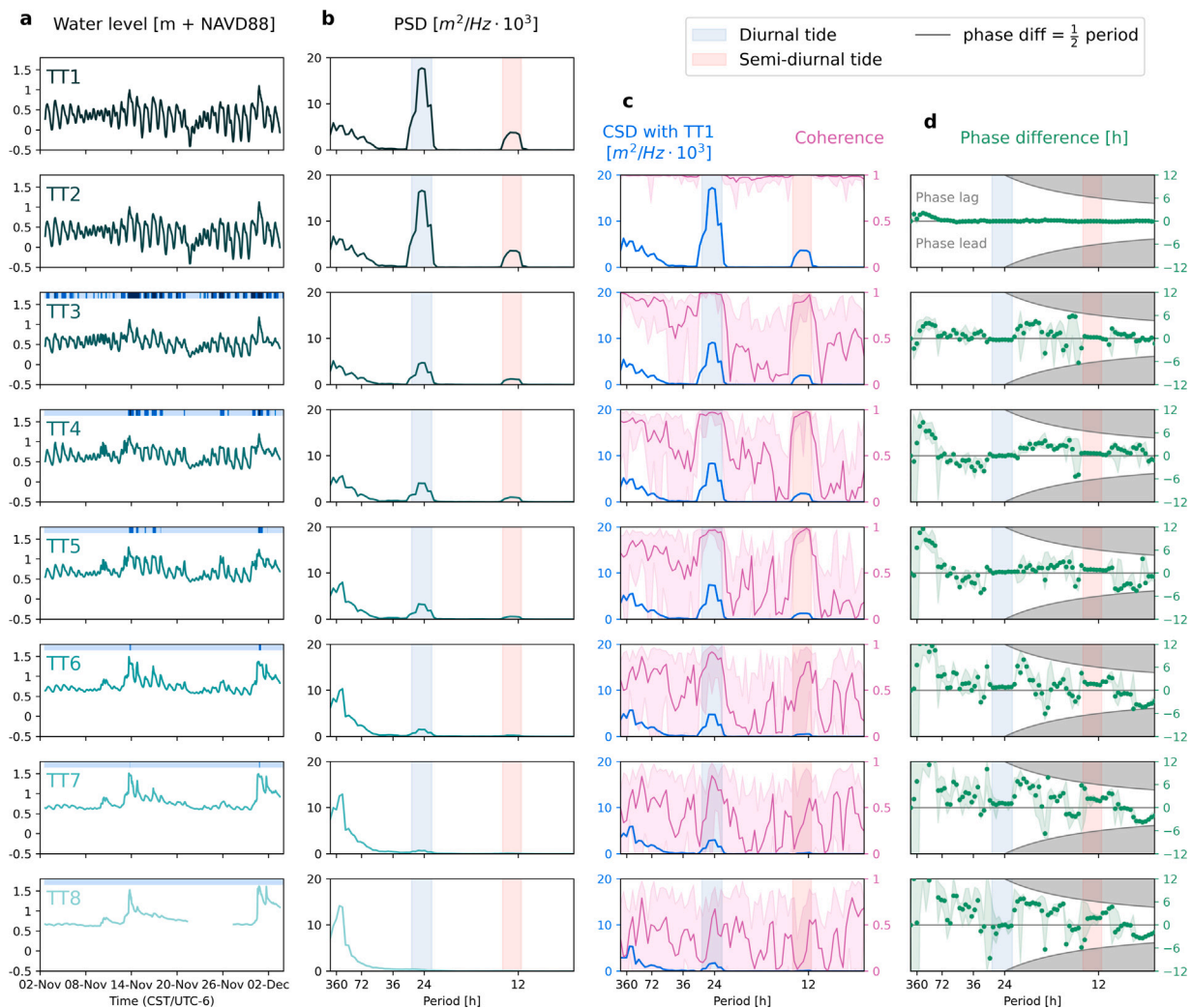


Fig. 5. Multitaper spectral analysis of the tidal propagation into along the stations at TT. (a) Observed water level time series at each station, with the blue shaded bar representing the inundation regime over time (see Fig. 3); (b) Power spectral density (PSD) computed from the detrended time series; (c) cross-spectral density (CSD, blue) and coherence (pink, 90% confidence interval given by shaded area) between station 1 and stations 2–8; (d) estimated phase difference (green) between station 1 and stations 2–8 in hours (uncertainty given as green shaded area). A positive (negative) phase difference denotes a lag (lead) in the signal at stations 2–8. The maximum phase difference (1/2 period) is denoted by the gray borders. In columns b–d, the tidal bandwidths are shaded in blue (diurnal) and red (semidiurnal). For location SW, see supplementary Figure S3.

3.2.2. Tide

The computed multitaper PSDs at each station showed clear peaks around the diurnal and semidiurnal tidal frequencies (Fig. 5b). As expected, the spectra at the foreshore stations (TT1 and TT2) were nearly identical, confirmed by the CSD and coherence which was near 1 across the frequency range (Fig. 5c). Towards the dune, the tidal signal decayed and the power shifted to lower frequencies. The tide already showed significant decay at stations 3–5, but the coherence remained near 1 over both tidal bandwidths, with relatively narrow 90% confidence intervals (low uncertainty). From TT6 on, most of the tidal power was damped out and the coherence dropped, with increasing uncertainty (confidence intervals). Nonetheless, the diurnal peak was still clear in the CSDs at stations 6–8. At TT8 the coherence was inconsistent across the frequency range and had no clear peaks around the tidal frequencies. This may be partly caused by the missing data between 21–28 November, as the tidal coherence at SW8 was higher and less uncertain (see supplementary Figure S3).

The total diurnal and semi-diurnal amplitudes computed from the PSDs amounted to 48 and 21 cm at TT1 and 47 and 24 cm at SW1, close to the predicted values of 42 and 21 cm at the NOAA Pleasure Pier station (Fig. 6). As expected, the amplitudes and phases at stations 1 and 2 were approximately equal. The amplitudes then rapidly decayed to below 10 cm at station 8—a reduction of 80%–85% at both TT and SW. The computed phase lags relative to station 1 were more inconsistent, but generally showed an increasing lag (nearly 2 h) towards the dune. The diurnal tide lagged less than the semi-diurnal tide. Uncertainty in the estimated phase lags also increased towards the dune, but was generally much lower within the tidal bands than outside.

It should be noted that, particularly for stations 3–5, the time series represent different water level regimes. Therefore, the computed amplitudes and phase lags do not represent pure groundwater signals and should be seen as an estimate of the conditions at that particular location across water level regimes. We therefore mainly describe the trends seen here, rather than absolute values. For instance, the results showed an unexpected, but small phase lead (15–20 min) for the diurnal tide at TT3 and SW3. However, these stations had the most

inconsistent water level regimes (see blue shaded bars in Fig. 5a). This lead is likely caused by noise or interference from other processes, as it should physically not be possible for the “groundwater” tide to lead the ocean tide (see also Section 4.1).

3.2.3. Surge and rainfall

Fig. 7 shows the low-passed time series along with the peaks of the five considered events. The Reverse surge (21/22 November) and Surge (25/26 November) were the only two events without rain. During the reverse surge, all backshore stations were in the groundwater regime and the amplitude quickly decayed from ≈ 0.55 m in the foreshore to < 0.2 m near the dune toe (Fig. 8). The smaller amplitude of the positive surge was relatively stable between stations 1–3 (≈ 0.15 m), then slightly increased at stations 4 and 5. Station 5 was the first station in the groundwater regime and from there, the amplitude decreased towards the dune toe, similarly to the reverse surge. Both events showed an increasing time lag of the peaks towards the dune, with the reverse surge showing a larger lag as it propagated a longer distance through the groundwater (up to 11–13 h, compared to 3–5 h for the positive surge, see Fig. 8).

The rain-only event (9/10 November) shows that rainfall can lead to a significant response in the low-passed time series, with amplitudes of about 0.1–0.25 m across the stations. There is also an increasing time lag of the low-pass rain peak between stations 3 and 8 at both locations. This does not represent a landward propagating signal—rather the time for the rain to infiltrate increases with the vertical distance to the GWT, which generally increases in landward direction (see also Section 4.1).

The two storm events (Storm 1 and Storm 2) consisted of positive surges (approximately 0.3 and 0.55 m, respectively, at station 1), accompanied by rainfall. During both events, the lower stations were fully inundated and the GWT at the upper stations reached the sand surface. For Storm 1, rainfall was persistent over the entire day (13 November) leading up to the surge peak, but less intense and there was no rain after the surge peak (Fig. 7c–e). The amplitude in the low-passed signal was relatively stable across the first three stations (≈ 0.3 m), before increasing up to 0.55–0.65 m at station 7, and decreasing

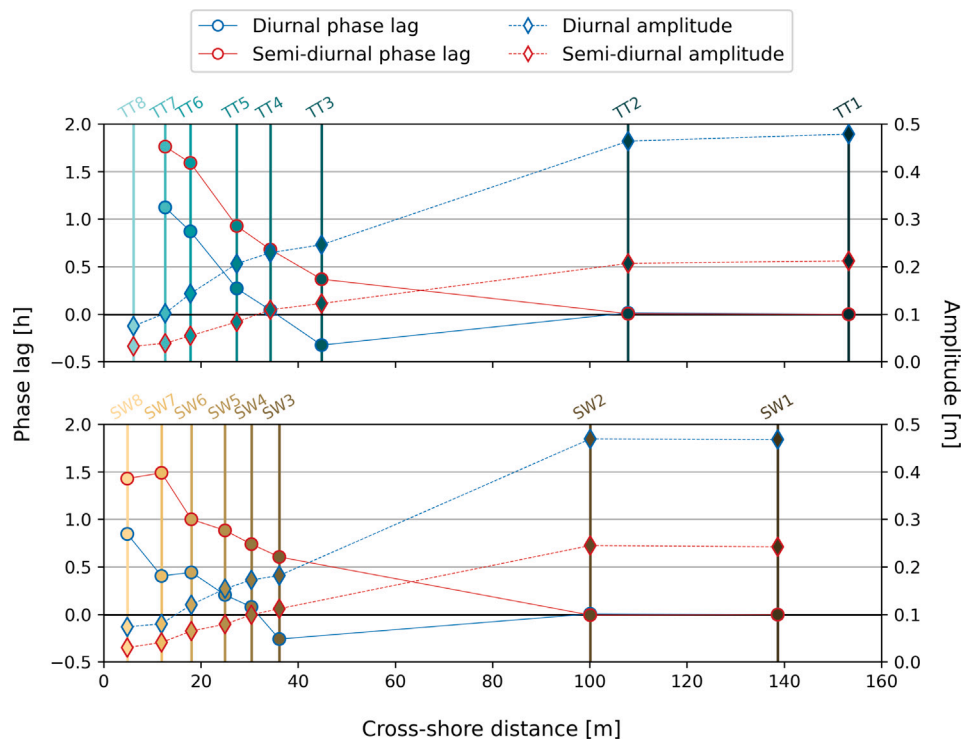


Fig. 6. Summary of tidal amplitudes (diamonds, right y-axis) and phase lags (circles, left y-axis) across the field stations of locations TT (a) and SW (b). The phase lags are given relative to station 1.

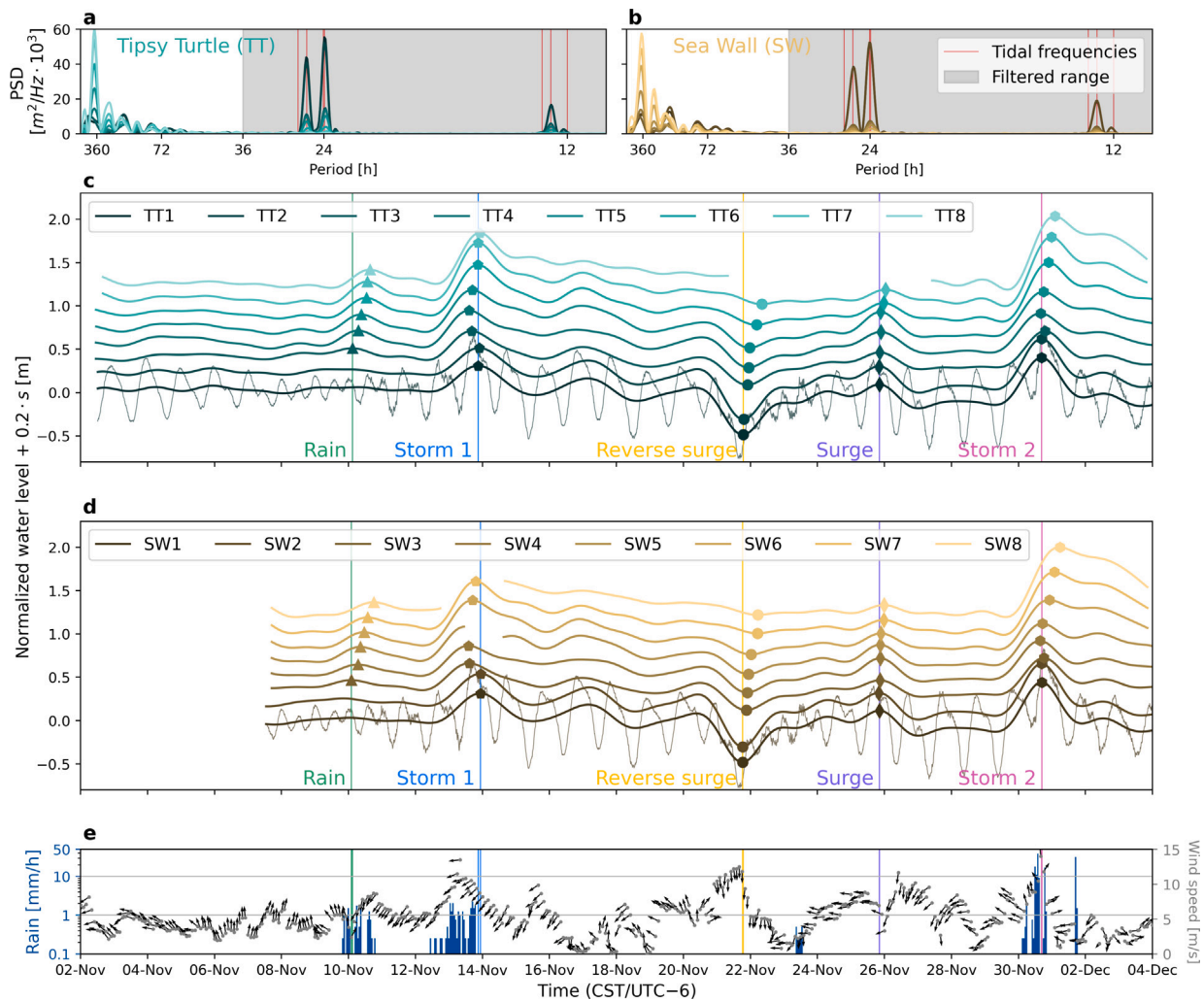


Fig. 7. (a, b) Power spectral densities (PSD) computed from single FFT's of the 10-min time series. The low-pass FFT filter removed all periods shorter than 36 h (gray-shaded area); (c), (d) Low-passed and normalized water level recorded at each station. The time series were shifted vertically in steps of 20 cm for visualization purposes. Markers track the extrema corresponding to five individual events: rain (triangles, green), storm 1 (pentagons, blue), reverse surge (circles, yellow), surge (diamonds, purple), and storm 2 (hexagons, pink). The colored vertical lines show the time of the extrema at station 1 (station 3 for rain); (e) Time series of hourly precipitation rates at the GLS weather station (blue bars), and 2-h averaged wind speeds (gray dots) and directions (black arrows) at the NOAA North Jetty station.

slightly at TT8 (there was no data for SW8, Fig. 8). For Storm 2 the rain was very intense (up to 50 mm/h at NWS GLS) but for a shorter period and closer to the peak of the surge. About one day after the peak surge there was another heavy shower (Fig. 7c–e). Moreover, the meteorological surge (± 0.55 m) was almost double that of Storm 1, leading to a stronger surge influence compared to the rain. The amplitude decreased at station 3 and then steadily increased to >0.8 m at station 8, although only at TT6, TT7, TT8, SW7, and SW8 was the amplitude larger than in the foreshore (Fig. 8).

The time lags during the two storms were more inconsistent than during the surge-only events. Storm 1 showed an apparent lead of the peak at the groundwater stations, compared to the foreshore surge. Especially the lower stations (3–5) showed large leads (up to 6 h at TT4 and 8 h at SW4). During Storm 2 the time lags were more in line with expectations, increasing towards the dune (up to 9–12 h at station 8). There were still small leads at TT4/SW4 (about 1 hour), even though at TT3/SW3 there was a lag. The phase leads are likely related to the response of the GWT to multiple driving processes acting simultaneously, notably the surge and rain (see Section 4.1). Next to the amplitude and phase changes across the stations, the peaks of the two storms also became increasingly asymmetric towards the dune toe, with the groundwater rising faster and dropping slower.

3.3. Nest flooding

The nest depth threshold was exceeded by the GWT several times at all upper groundwater stations (6–8) of both TT and SW (Fig. 9). The total number of flooding events was highest at TT6 (7) and SW6 (14) and decreased towards the dune toe, with 3 and 2 flooding events observed at TT8 and SW8, respectively (Table 3). At all six stations, there was at least one inundation event that lasted between 12 and 24 h, and all three SW stations had one event lasting more than 24 h. At both sites, the longest inundation events happened during the storm on 30 November. Flooding events generally lasted for longer at SW than at TT. The storm on 30 November was followed by another heavy rain shower on 1 December (Fig. 7e). At SW6 and SW7, the water level did not drop below the threshold before rising again due to the additional rainfall, leading to flooding events of about 70 and 60 h, respectively. At TT6, about 25 cm of the beach surface was eroded after the first storm (13 November), meaning that any potential nests would have likely been washed away. At the other stations, morphological changes were milder (5–10 cm) and generally showed more accretion than erosion.

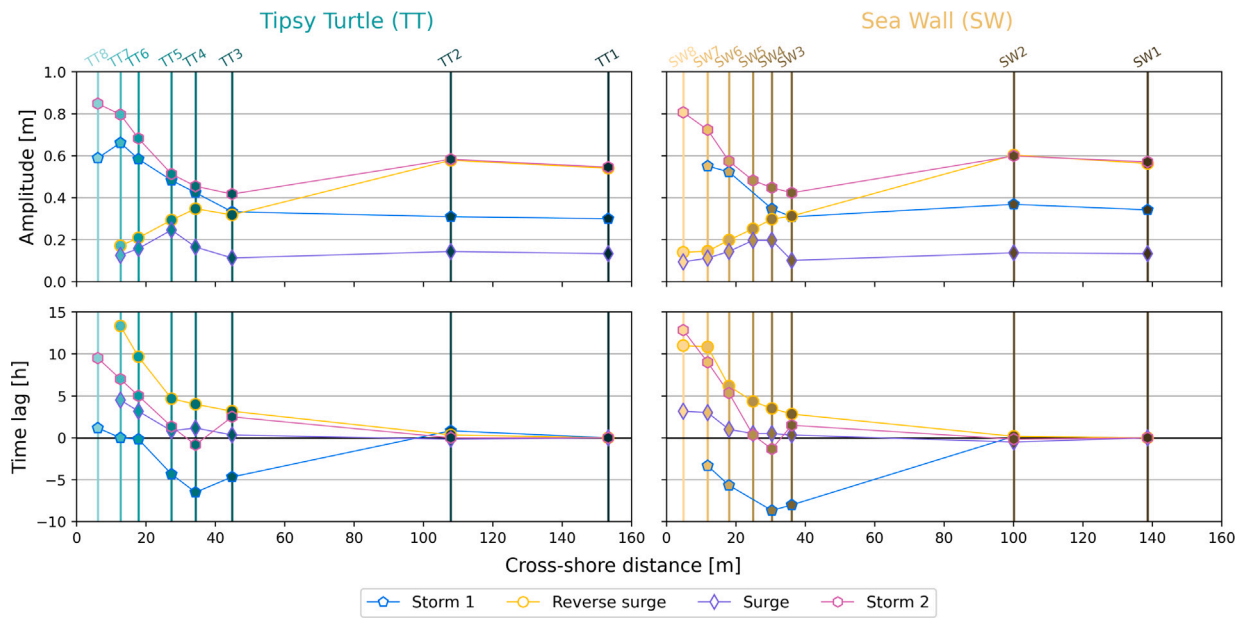


Fig. 8. Estimated amplitudes (top row) and time lags (bottom row) of the extrema of the five considered events at TT (left column) and SW (right column).

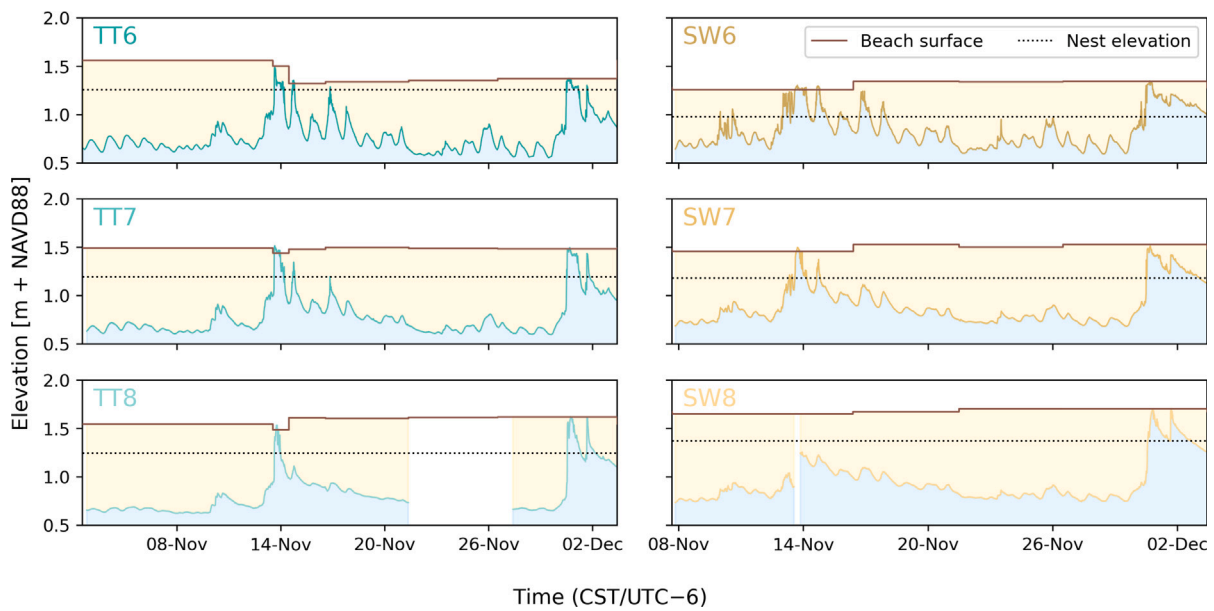


Fig. 9. Overview of observed GWTs at stations 6–8 at TT (left) and SW (right). The beach surface and typical Kemp’s Ridley nest depth are added for reference.

Table 3

Overview of nest flooding events at the upper groundwater stations, divided into bins depending on the flooding duration.

Duration [h]	TT6	TT7	TT8	SW6	SW7	SW8
<3	4	2		6	2	
3–6		1		4	1	
6–12	2		1			
12–24	1	2	2	3	1	1
>24				1	1	1
Total #	7	5	3	14	5	2

4. Discussion

4.1. Groundwater response to driving processes

In line with previous studies on beach groundwater (e.g., Cartwright et al., 2004; Hegge and Masselink, 1991; Nielsen, 1990; Raubenheimer

et al., 1999; Turner and Nielsen, 1997), our results show that the beach matrix acts like a low-pass filter, increasingly damping out higher frequency fluctuations in the groundwater. The observed super-elevation (0.5–0.6 m) and vertical variability of GWTs ($O(1\text{ m})$) are also consistent with previous observations reported in the literature (e.g., Housego et al., 2021; Nielsen, 1990; Turner et al., 1997). IG waves appear to be relevant near the swash zone, where they shoal before reaching the shore, also in line with previous studies (e.g., van Dongeren et al., 2007; Henderson and Bowen, 2002; Thomson et al., 2006). Only the lower frequency IG bands propagate into the GWT, shown by a bimodal behavior of the mean IG period across groundwater and mixed/submerged conditions. The tidal signal becomes increasingly damped, asymmetric, and phase-lagged towards the dune toe. Both IG and tidal fluctuations are damped to a degree that they have little influence on the GWT near the dune toe. Hence, of the considered processes, the surge and rainfall dominate the observed GWT fluctuations in the upper backshore, including the nesting area.

As multiple driving processes simultaneously interact with the beach matrix, their combined effects result in a conditional GWT response. During storm 1 the ocean surge peak occurred on the falling tide, whereas during storm 2 it occurred on the rising tide, much closer to the high tide. This partly explains the higher water levels observed during storm 2. Rainfall and bed level also contribute, particularly because they often coincide with stormy conditions (Zheng et al., 2013), as was the case during both observed storms. The GWT time series represent the combined response to all these processes, making it difficult to isolate the signals of individual drivers, in particular those acting on similar time scales. More advanced methods which work better on non-stationary data, such as wavelet analysis or empirical mode decomposition, could potentially improve the isolation of the surge, for example. Another approach could be to assess the surge component and overheight using an empirical or analytical model (e.g., Li et al., 2004; Nielsen, 1990, 1999). Moreover, longer-term observations (6+ months) would enable more detailed analysis as they facilitate more accurate spectral estimation and increase the chance of capturing isolated events (e.g., high waves but no significant surge, or vice versa).

This combined response to multiple simultaneous drivers may explain some of the limitations and inaccuracies in our analyses. For instance, the observed time leads of the groundwater peaks relative to the surge peaks in the foreshore during the storm events (Fig. 8). Both storm events were accompanied by rainfall and high wave runoff. Before the surge peak of storm 1 (13 Nov) there was a ± 24 -h period with several rain showers, elevating the GWT ahead of the surge (Fig. 10a). Consequently, as the surge and tide increase and wave runoff reaches further up the beach, the GWT may reach the beach surface before the peak of the foreshore water level. Unless the location is fully submerged thereafter, the GWT will not rise further, resulting in an

earlier low-pass peak. These hypotheses are supported by the second storm (30 Nov) showing mostly time lags, as the rain, ocean surge, and high tide are more in-sync (Fig. 10b). Finally, bed level changes complicated things even further as they changed the potential extent of the GWT. For instance, erosion can lower the beach surface and, with it, the GWT (e.g., at TT5 and TT6 during both storms 10a,b). As such, the GWT can sometimes even be used to roughly track morphological changes (Anarde et al., 2020).

The anomalous phase lead of the diurnal tide at TT3 and SW3 (Fig. 6) is likely the result of noise or interference from surface flows (e.g., during the storms). Both stations were regularly submerged (Fig. 3). During submergence no significant time difference in the tidal signal is expected. However, once the beach re-emerges the sediment damps and slows the tidal retreat in the GWT. This creates a time-varying asymmetry in the signal, as the low tides occurred during groundwater conditions (and therefore lag the ocean tide), whereas many high tides occurred in mixed/submerged conditions (Fig. 10c). In some cases, the groundwater may reach the beach surface ahead of the high tide peak and, if the location is not submerged, stop rising until the tide drops again, which might translate to a phase lead. However, this is unlikely to completely offset the observed lags in the low tide and therefore fails to explain the phase leads. These could also be an artifact of the spectral analysis being applied to the full time series with mixed regimes, essentially violating the stationarity condition, even though the ocean tidal signal itself is inherently stationary. The computed amplitudes and phase differences shown in Fig. 6 should therefore not be used as absolute values but rather to identify patterns (e.g., overall increasing lag towards dune).

The full response of the GWT to rain cannot be assessed from the low-passed time series because the main response occurs on shorter

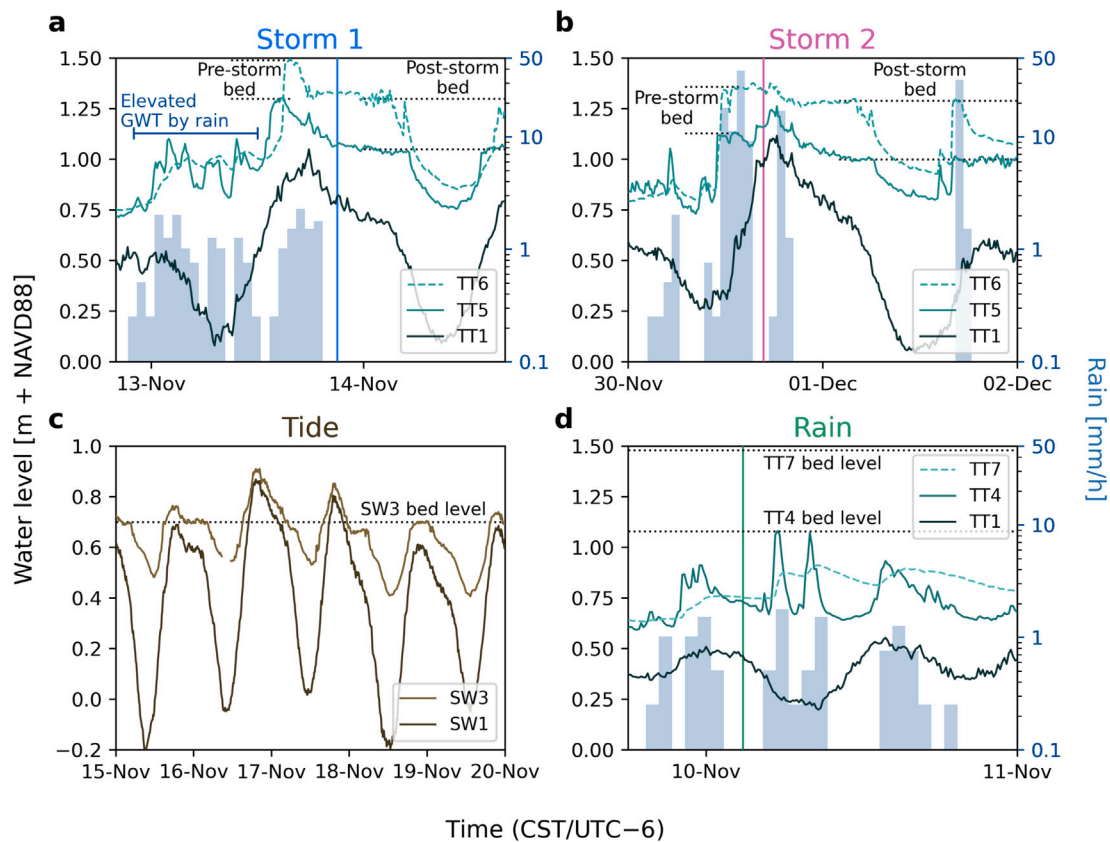


Fig. 10. Observed (ground)water levels at various stations, showing the conditional GWT response to the driving processes and their interaction with the beach matrix. (a) Water levels and bed level changes at TT during Storm 1; (b) Water levels and bed level changes at TT during Storm 2; (c) Tidal damping and asymmetry at SW3 compared to SW1; (d) GWT response to rain at TT on 9/10 November. Black dotted lines indicate bed levels, while the blue, pink, and green vertical lines indicate the time of the low-frequency peak at TT1 (Storm 1 and Storm 2) and TT3 (Rain), see also Fig. 7.

timescales. The rain event on 9/10 November consisted of several showers over a period of about one day, leading to multiple short peaks in the GWT (Fig. 10d). These are smoothed into one peak in the low-passed time series, but the GWT response occurs at higher frequencies. At stations 3–5 the response was different compared to stations 6–8, with two clear spikes indicating a relatively quick uprush of the GWT, before rapidly dropping again. At stations 6–8 the response was more gradual and the GWT also dropped more slowly, failing to reach its pre-shower level before the next increase. This difference is likely due to the sediment above the GWT being more saturated at the lower stations, reducing the effective porosity, and allowing the infiltrating rain to fill the pores more rapidly. Moreover, before the first shower, the GWT is about 45 cm below the surface at TT4 compared to about 85 cm at TT7 (Fig. 10d). Therefore, the water needs to infiltrate further down at the higher stations and will get absorbed into the pore spaces of the drier sand, smoothing the response and leading to a time delay, which ultimately shows in the low-passed peak as well. Local and more frequent measurements of rainfall at the study site could help better identify and describe the GWT response to rain.

4.2. Impact on nest flooding

Our results suggest that the surge and rainfall are the dominant drivers of nest flooding on Galveston's beaches and that the nest threshold was breached several times at each station. Past studies have indicated that both the frequency and duration of flooding events are critical for egg viability. For example, turtle eggs have been reported to tolerate short inundation periods (1–3 h), but egg mortality rates start to increase quickly after six hours (Pike et al., 2015). Moreover, eggs in the first or last 20% of their incubation periods are practically intolerant to flooding of any duration, with hatching rates already decreasing drastically after inundations as short as one hour, especially for saltwater (Limpus et al., 2021). Rainfall by itself likely has less impact on turtle nests than the surge, as eggs are more tolerant to freshwater and showers often lead to high but relatively short spikes in the GWT. A high surge on the other hand is bound to elevate the GWT for at least several hours, especially in combination with wave runoff. However, compound events, like the rain-elevated GWT ahead of the surge during storm 1 still make rain an important factor for nest flooding.

The observed frequency and duration of flooding events in this study make it highly unlikely that turtle nests on Galveston Island's beaches could yield viable hatchlings (Table 3). The GWT is relatively high, generally staying within 1 m of the sand surface, and can rise quickly and for prolonged time periods. We believe that this is due to a combination of the local sediment characteristics and the mild-sloping, low-elevation beach and dune system. Kemp's ridleys sometimes also nest on or behind the first dune (Marquez, 1994), potentially to mitigate nest flooding. We did not monitor the GWT beyond the dune toe, however, the low elevation of the first "dune" (usually below 1 m) makes it unlikely that those nests would be safe from inundation. Moreover, we used a relatively shallow nest threshold—in reality nests can be deeper (especially for other species), thus experiencing more flooding if laid in the same region of the beach. Our findings indicate that Galveston Island's beaches currently do not provide an ideal nesting habitat for sea turtles, even for relatively shallow nests (we did not quantitatively evaluate deeper nest thresholds as these would have been inundated even longer). Therefore, we recommend continuation of the relocation practices carried out by the State of Texas, as implemented by the state sea turtle coordinator and the Padre Island National Seashore's Division of Sea Turtle Science and Recovery.

Moreover, we hypothesize that the CF could similarly disrupt egg gas exchange, leading to mortality rates comparable to GWT inundation. Here, we define the CF as the fully saturated zone above the GWT (it is sometimes also defined as the full zone of capillary

action, reaching into the partially saturated zone with increased oxygen availability). Oxygen availability rapidly decreases in the fully saturated CF, suggesting that gas exchange for eggs within that zone may be insufficient (Haberer et al., 2014; Jost et al., 2011). Especially in fine sediments (<0.1 mm), the CF width may potentially exceed 0.7 m (Turner and Nielsen, 1997). Unfortunately, our deployed moisture sensors were not calibrated properly, and we could not quantitatively estimate the CF from the measurements (Christiaanse et al., 2025). However, a rough estimate of the CF width may be obtained from the average grain size: using $D_{50} \approx 0.15$ mm for Galveston Island (Christiaanse et al., 2025) would result in a theoretical CF in the order of 0.5 m (Turner and Nielsen, 1997). This could drastically reduce the suitability of Galveston Island's beaches for turtle nesting. Thus, despite the absence of existing literature on how the CF might impact sea turtle nests, we believe that it could be a significant determinant for turtle nests. While gas exchange is important, sea turtle eggs also need sufficient moisture levels (Ackerman, 1997; Mortimer, 1990), suggesting they could be optimally placed in the partially saturated zone above the CF. Future research should therefore not only investigate the tolerance of turtle nests to complete inundation but also to CF exposure, for example by extending field/laboratory experiments like Limpus et al. (2021) and Pike et al. (2015). Additionally, simultaneous measurements of CF extent and nest depths could shed more light on a potential relation and optimal nest depths.

The beach groundwater dynamics during the nesting season (April–September) may differ to some degree from our observations (mainly November). For instance, the higher summer temperatures may lead to more evapotranspiration (i.e., faster drying of the beach), and therefore a lower mean GWT. However, hourly water levels at NOAA's North Jetty station from 2001–2023 indicate that extreme water levels are more common and reach significantly higher values (>1.5 m NAVD88) during the nesting season (Fig. 11a). This is most likely due to the peak of the hurricane season (August–October) overlapping with nesting. Major hurricanes would completely wash away any nests, but regular (tropical) storms may frequently bring similar or slightly higher water levels than those observed in November 2023. The North Jetty water levels are relatively representative of those observed at TT1, though TT1 shows higher extremes, likely owing to wind and wave setup (Fig. 11b). Long-term rainfall data from GLS (1991–2020) suggest that while the early nesting season is drier than November, August and September are wetter (Fig. 11c). Based on these factors, we expect the risk of nest flooding to be similar or even higher during the nesting season. Long-term observations of the GWT combined with measurements of local rainfall and evapotranspiration would help validate this hypothesis by improving our understanding of the steady state groundwater flow and seasonal GWT variations.

We chose the two field sites for this study because they facilitated comparisons between a more natural (TT) and engineered (SW) beach setting. While the general results were similar, the engineered SW site typically exhibited a higher GWT, slower drainage, and longer flooding durations, even though the beach elevation at SW7 and SW8 was slightly higher than at TT7 and TT8. This is likely the result of an interplay of various factors, which may include the engineered beach setting at SW. For example, the profile at TT (including the berm that eroded during storm 1) may be more effective in preventing higher water levels from affecting the GWT in the nesting area. Varying sediment characteristics may also play a role, for instance nourished beaches can be more compacted than natural ones (Hannides et al., 2019), which would result in lower permeability and slower groundwater drainage. Although nourishments in Galveston have generally been placed south of SW, the sand was still more compacted than at TT and contained visibly more shelly material (Christiaanse et al., 2025). The sea wall, paved street, and groins may also affect groundwater flow and rainwater runoff in the area. For example, the sea wall foundation could present a significant obstacle to groundwater drainage towards the landward side. Although both sites are currently not ideal

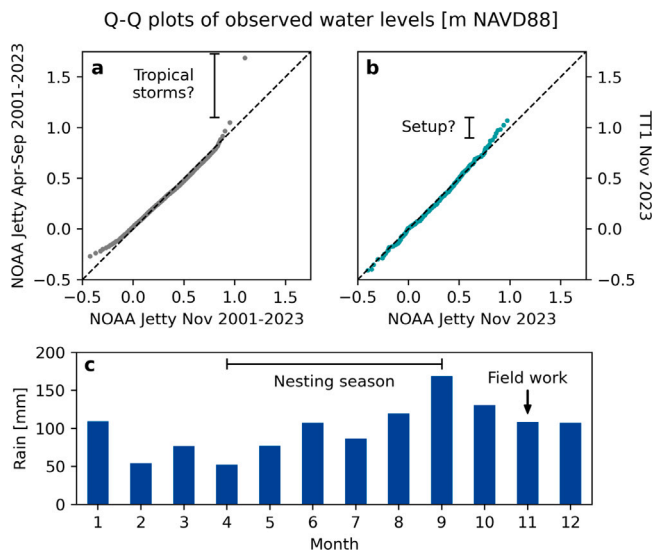


Fig. 11. Statistical comparison of water levels and monthly rainfall during the nesting season (April–September) and November. (a) Quantile-Quantile (Q-Q) plot of the observed hourly water level at the NOAA North Jetty station in November 2001–2023 (x-axis) and April–June 2001–2023 (y-axis). (b) Q-Q plot of the observed water levels in November 2023 at NOAA Jetty (x-axis) and TT1 (y-axis). (c) NCEI Climate Normals mean monthly precipitation totals over 1991–2020 at the GLS weather station.

for nesting, our observations indicate that the engineered site (SW) is less suitable than the natural one (TT). This supports previous studies that have observed reduced sea turtle nesting suitability on nourished beaches (e.g., Brock et al., 2009; Grain et al., 1995; Steinitz et al., 1998).

Given the interdependence between groundwater dynamics and beach slope, elevation, and sediment size (Turner et al., 1997), the importance of GWT fluctuations for nest flooding may vary significantly among global sea turtle nesting beaches. Specifically, steeper, higher elevation beaches with coarser sediments typically have greater permeability and drainage (Turner et al., 1997), meaning that the mean GWT is likely deeper below the surface and the CF width is smaller (Turner and Nielsen, 1997). In such environments, we do not expect such frequent and extended periods of elevated groundwater, and therefore also less risk of prolonged nest inundation. That is, nests may still flood during high wave or surge events, but if the GWT drops below the nests more quickly the risk to egg viability will be lower. Nonetheless, continued inundation of nests is a threat on many nesting beaches worldwide, including the largest existing green turtle rookery on Raine Island, Australia (Limpus et al., 2021). Moreover, Kemp's ridleys are the smallest species of sea turtle, digging the shallowest nests. Other species can dig deeper nests (up to about 1 m below the surface), which may remain inundated for longer time periods, depending on their location in the beach profile. Therefore, while flooding is primarily driven by ocean processes (and rain), our results underscore the importance of considering the GWT in studies and assessments of nest inundation, particularly in low-elevation beach systems. In that context, future research should work towards developing a generic framework to assess nest inundation on sandy beaches, taking into account local beach morphology and aquifer properties, hydrological and hydrodynamic forcing, and groundwater dynamics.

4.3. Towards nature-based solutions that enable sea turtle nesting

While it remains uncertain how sea turtles select their nesting beaches (Miller et al., 2003), it has been hypothesized that they try to reduce the risk of nest flooding by nesting in regions with lower tidal ranges and lower extreme surges (Christiaanse et al., 2024),

and selecting an appropriate spot or elevation on the beach (Maurer and Johnson, 2017). Coarser grain sizes are generally correlated with steeper beach slopes (Bujan et al., 2019), and have greater permeability, resulting in faster groundwater drainage (Turner et al., 1997) and a thinner CF (Turner and Nielsen, 1997). Based on these relations and our observations in a fine-grained, low-elevation beach system, we would expect sea turtles to favor higher-elevation beaches with coarser sediment. Beach elevation has previously been identified as an important factor in determining nesting suitability for Kemp's ridleys specifically (Culver et al., 2020), but also loggerhead, hawksbill, and green turtles (e.g., Horrocks and Scott, 1991; Kikukawa et al., 1999; Yamamoto et al., 2012). Yet, to date no clear relationship between sediment size and turtle nesting has been found (e.g., Foley et al., 2006; Mortimer, 1990), except that turtles appear to avoid sites with extremely high or low grain sizes (Yamamoto et al., 2012). Mortimer (1990) hypothesized that too low water content could explain green turtles struggling on beaches with coarse sand (± 1 mm), but did not conclude anything for finer grain sizes.

Beach elevation will become even more important in the light of future sea level rise, as the mean GWT is expected to follow mean sea level (Bjerkli et al., 2012; Michael et al., 2013). This will increase the risk of elevated groundwater due to ocean- and/or rain-driven inundation if the beach morphology cannot keep up with the rising water levels. This is particularly concerning in regions with high relative sea level rise rates, like the western Gulf of Mexico. However, it may also provide opportunities for nature-based solutions to improve the suitability of low-lying beach systems for turtle nesting—for instance, by increasing the beach elevation through turtle-friendly beach nourishments. Different beach nourishment strategies for Galveston Island are currently being evaluated for coastal resilience and protection (USACE, 2021) and these studies should include the impact on turtle nesting and the flooding of nests in particular. Increasing the beach elevation through re-profiling or nourishment has previously been suggested as a nature-based solution for nesting beach rehabilitation (Limpus et al., 2021; Montague, 1993) and has successfully been implemented on Raine Island, Australia, in the past decade (Smithers and Dawson, 2023). However, a lot of care must be taken to ensure that the resulting beach profile and sediment characteristics enable turtle nesting, rather than hindering it (e.g., by nourishing with native sediment and reducing sand compaction; Grain et al., 1995; Hannides et al., 2019; Montague, 1993).

5. Conclusion

Understanding how ocean processes and rain drive short-term beach groundwater variability in sea turtle nesting areas is critical for evaluating management practices like nest relocation and designing nature-based solutions that mitigate nest flooding. In this study, we investigated the beach GWT response to ocean processes and rain in a fine-grained, mild-sloping beach system by analyzing field data gathered on Galveston Island, Texas in the fall of 2023. We quantified the influence of IG waves, tide, surge, and rainfall on short-term GWT fluctuations between the high tide line and the dune toe by performing tailored spectral analyses on ± 30 -day time series of water level observations, categorized into *groundwater*, *mixed*, and *submerged* regimes.

We observed significant short-term variability in the beach GWT across the backshore ($O(1$ m)). Our results were generally consistent with previous studies, showing that the beach matrix acts as a low-pass filter, with higher frequency signals getting increasingly damped, lagged, and distorted landward. Surge and rainfall dominated the GWT response in the upper backshore, the primary sea turtle nesting zone. The tidal signal was increasingly damped and asymmetric towards the dune, whereas IG waves were only relevant near the swash zone. Our analysis explicitly excluded inland groundwater processes (e.g., aquifer

recharge or regional groundwater flow), focusing solely on ocean and rainfall-driven groundwater fluctuations within the beach.

A flooding threshold based on a representative nest depth of 30 cm below the surface revealed multiple, prolonged nest inundation events (exceeding 12 h), even for the shallowest nests. This suggests that Galveston Island is currently not a suitable nesting habitat for sea turtles as nests are likely to get flooded frequently and for prolonged periods. We therefore recommend continuing the current nest relocation program. Our findings underscore the importance of including the GWT in studies of nest flooding and encourage further research towards nature-based solutions that enable sea turtle nesting in low-elevation beach systems like Galveston Island, for example through the design of turtle-friendly nourishments. By integrating insights from coastal science and sea turtle biology, we can develop tailored solutions that not only mitigate flooding risks but also enhance habitat suitability under future climate scenarios.

CRedit authorship contribution statement

Jakob C. Christiaanse: Writing – review & editing, Writing – original draft, Visualization, Validation, Software, Resources, Methodology, Investigation, Funding acquisition, Formal analysis, Data curation, Conceptualization. **José A.A. Antolínez:** Writing – review & editing, Supervision, Resources, Investigation, Funding acquisition, Conceptualization. **Christopher D. Marshall:** Writing – review & editing, Resources. **Jens Figlus:** Writing – review & editing, Resources, Investigation. **Timothy M. Dellapenna:** Writing – review & editing, Resources. **Ad J.H.M. Reniers:** Writing – review & editing, Supervision, Formal analysis.

Declaration of competing interest

The authors declare that they have no known competing financial interests or personal relationships that could have appeared to influence the work reported in this paper.

Acknowledgments

The data analyzed in this paper was collected as part of the TURTLE project, which is funded by TKI Delta Technology (grant number T-DEL/2023/095) with support from TU Delft, Texas A&M University, Deltares, Boskalis, University of Exeter, and King Abdullah University of Science and Technology (KAUST). We would like to express our gratitude to the following people who contributed significantly to the data collection: Ir. Meve van der Grinten, Ir. Falco Taal, Dr. Nick Cohn, and Dr. Pete Tereszkiwicz. Further, we want to thank Prof. dr. Ian Turner and Dr. Marie-Pierre Delisle for discussing the data with us and sharing their thoughts and ideas. Finally, many thanks to Prof. dr. ir. Stefan Aarninkhof for his help with the funding acquisition.

Appendix A. Supplementary data

Supplementary material related to this article can be found online at <https://doi.org/10.1016/j.coastaleng.2025.104795>.

Data availability

All field data used in this study is described in Christiaanse et al. (2025) and available through the 4TU.ResearchData repository at: <https://doi.org/10.4121/93256801-e001-4627-9e49-8607967a0853>.

References

- Ackerman, R.A., 1997. The nest environment and the embryonic development of sea turtles. In: Lutz, P.L., Musick, J.A. (Eds.), *The Biology of Sea Turtles*. Vol. 1, CRC Press, Boca Raton, pp. 83–106.
- Anarde, K., Figlus, J., Sous, D., Tissier, M., 2020. Transformation of infragravity waves during Hurricane Overwash. *J. Mar. Sci. Eng.* 8 (8), 545. <http://dx.doi.org/10.3390/jmse8080545>.
- Babadi, B., Brown, E.N., 2014. A review of multitaper spectral analysis. *IEEE Trans. Biomed. Eng.* 61 (5), 1555–1564. <http://dx.doi.org/10.1109/TBME.2014.2311996>.
- Battjes, J.A., Bakkenes, H.J., Janssen, T.T., van Dongeren, A.R., 2004. Shoaling of subharmonic gravity waves. *J. Geophys. Res.: Ocean.* 109 (C2), <http://dx.doi.org/10.1029/2003JC001863>.
- Bauer, B., Davidson-Arnott, R., Hesp, P., Namikas, S., Ollerhead, J., Walker, I., 2009. Aeolian sediment transport on a beach: Surface moisture, wind fetch, and mean transport. *Geomorphology* 105 (1–2), 106–116. <http://dx.doi.org/10.1016/j.geomorph.2008.02.016>.
- Bear, J., Cheng, A.H.-D., Sorek, S., Ouazar, D., Herrera, I. (Eds.), 1999. *Seawater intrusion in coastal Aquifers — Concepts, methods and practices. Theory and Applications of Transport in Porous Media*, vol. 14, Springer Netherlands, Dordrecht, <http://dx.doi.org/10.1007/978-94-017-2969-7>.
- Befus, K.M., Barnard, P.L., Hoover, D.J., Finzi Hart, J.A., Voss, C.I., 2020. Increasing threat of coastal groundwater hazards from sea-level rise in California. *Nat. Clim. Chang.* 10 (10), 946–952. <http://dx.doi.org/10.1038/s41558-020-0874-1>.
- Bertin, X., de Bakker, A., van Dongeren, A., Coco, G., André, G., Arduin, F., Bonneton, P., Bouchette, F., Castelle, B., Crawford, W.C., Davidson, M., Deen, M., Dodet, G., Guérin, T., Inch, K., Leckler, F., McCall, R., Muller, H., Olabarrieta, M., Roelvink, D., Ruessink, G., Sous, D., Stutzmann, E., Tissier, M., 2018. Infragravity waves: From driving mechanisms to impacts. *Earth-Sci. Rev.* 177, 774–799. <http://dx.doi.org/10.1016/j.earscirev.2018.01.002>.
- Bjerklie, D.M., Mullaney, J.R., Stone, J.R., Skinner, B.J., Ramlow, M.A., 2012. Preliminary Investigation of the Effects of Sea-Level Rise on Groundwater Levels in New Haven, Connecticut. Technical Report, U.S. Geological Survey Open-File Report 2012-1025, <http://dx.doi.org/10.3133/OFR20121025>.
- Brock, K.A., Reece, J.S., Ehrhart, L.M., 2009. The effects of artificial beach nourishment on marine turtles: Differences between loggerhead and green turtles. *Restoration Ecol.* 17 (2), 297–307. <http://dx.doi.org/10.1111/j.1526-100X.2007.00337.x>.
- Bronze, T., 1992. On the performance advantage of multitaper spectral analysis. *IEEE Trans. Signal Process.* 40 (12), 2941–2946. <http://dx.doi.org/10.1109/78.175738>.
- Bujan, N., Cox, R., Masselink, G., 2019. From fine sand to boulders: Examining the relationship between beach-face slope and sediment size. *Mar. Geol.* 417, 106012. <http://dx.doi.org/10.1016/j.margeo.2019.106012>.
- Capuano, R.M., Jones, C.R., 2022. Clay-cation composition of river sediments as evidence of wet versus dry paleoclimate. *Appl. Geochem.* 146, 105421. <http://dx.doi.org/10.1016/j.apgeochem.2022.105421>.
- Carpio Camargo, A.J., Álvarez Gutiérrez, Y., Jaramillo Véliz, J., Sánchez Tortosa, F., 2020. Nesting failure of sea turtles in Ecuador - causes of the loss of sea turtle nests: the role of the tide. *J. Coast. Conserv.* 24 (5), 55. <http://dx.doi.org/10.1007/s11852-020-00775-3>.
- Cartwright, N., Nielsen, P., Li, L., 2004. Experimental observations of watertable waves in an unconfined aquifer with a sloping boundary. *Adv. Water Resour.* 27 (10), 991–1004. <http://dx.doi.org/10.1016/j.advwatres.2004.08.006>.
- Caut, S., Guirlet, E., Girondot, M., 2010. Effect of tidal overwash on the embryonic development of leatherback turtles in French Guiana. *Mar. Environ. Res.* 69 (4), 254–261. <http://dx.doi.org/10.1016/j.marenvres.2009.11.004>.
- Christiaanse, J.C., Antolínez, J.A.A., van der Grinten, M.J., Taal, F., Figlus, J., Dellapenna, T.M., Ritt, B., Marshall, C.D., Tereszkiwicz, P.A., Cohn, N., Majzlik, E.J., Reniers, A.J.H.M., 2025. Measurements of groundwater, hydrodynamics, and sand characteristics at a dissipative sea turtle nesting beach. *Sci. Data* 12 (1), 123. <http://dx.doi.org/10.1038/s41597-025-04455-5>.
- Christiaanse, J.C., Antolínez, J.A.A., Luijendijk, A.P., Athanasiou, P., Duarte, C.M., Aarninkhof, S., 2024. Distribution of global sea turtle nesting explained from regional-scale coastal characteristics. *Sci. Rep.* 14 (1), 752. <http://dx.doi.org/10.1038/s41598-023-50239-5>.
- Christiansen, M.J.A., Smulders, F.O.H., Vonk, J.A., Becking, L.E., Bouma, T.J., Engel, S.M., James, R.K., Nava, M.I., de Smit, J.C., van der Zee, J.P., Palsbøll, P.J., Bakker, E.S., 2023. Seagrass ecosystem multifunctionality under the rise of a flagship marine megaherbivore. *Global Change Biol.* 29 (1), 215–230. <http://dx.doi.org/10.1111/gcb.16464>.
- Culver, M., Gibeau, J.C., Shaver, D.J., Tissot, P., Starek, M., 2020. Using lidar data to assess the relationship between beach geomorphology and Kemp's Ridley (*Lepidochelys kempii*) nest site selection along Padre Island, TX, United States. *Front. Mar. Sci.* 7, 214. <http://dx.doi.org/10.3389/fmars.2020.00214>.
- de Vriend, H.J., van Koningsveld, M., Aarninkhof, S.G., de Vries, M.B., Baptist, M.J., 2015. Sustainable hydraulic engineering through building with nature. *J. Hydro-Environ. Res.* 9 (2), 159–171. <http://dx.doi.org/10.1016/j.jher.2014.06.004>.
- Delisle, M.-P.C., Kim, Y., Gallien, T.W., 2023. A numerical study of dam-break driven swash and beach groundwater interactions. *J. Geophys. Res.: Ocean.* 128 (9), <http://dx.doi.org/10.1029/2022JC019615>.

- van Dongeren, A., Battjes, J., Janssen, T., van Noorloos, J., Steenhauer, K., Steenbergen, G., Reniers, A., 2007. Shoaling and shoreline dissipation of low-frequency waves. *J. Geophys. Res.: Ocean.* 112 (C2), <http://dx.doi.org/10.1029/2006JC003701>.
- Foley, A.M., Peck, S.A., Harman, G.R., 2006. Effects of sand characteristics and inundation on the hatching success of Loggerhead Sea Turtle (*Caretta caretta*) clutches on Low-Relief Mangrove Islands in Southwest Florida. *Chelonian Res. Found. Turt. Conserv.* 5 (1), 32–41. [http://dx.doi.org/10.2744/1071-8443\(2006\)5\[32:EOSCAI\]2.0.CO;2](http://dx.doi.org/10.2744/1071-8443(2006)5[32:EOSCAI]2.0.CO;2).
- Gammon, M., Whiting, S., Fossette, S., 2023. Vulnerability of sea turtle nesting sites to erosion and inundation: A decision support framework to maximize conservation. *Ecosphere* 14 (6), e4529. <http://dx.doi.org/10.1002/ecs2.4529>.
- Garner, L.E., 1997. Geologic history, depositional environment, processes, and hydrology of Galveston Island, Texas. Bureau of Economic Geology, University of Texas at Austin, <http://dx.doi.org/10.26153/tsw/51702>.
- Gillham, R., 1984. The capillary fringe and its effect on water-table response. *J. Hydrol.* 67 (1–4), 307–324. [http://dx.doi.org/10.1016/0022-1694\(84\)90248-8](http://dx.doi.org/10.1016/0022-1694(84)90248-8).
- Gourlay, M., 1992. Wave set-up, wave run-up and beach water table: Interaction between surf zone hydraulics and groundwater hydraulics. *Coast. Eng.* 17 (1–2), 93–144. [http://dx.doi.org/10.1016/0378-3839\(92\)90015-M](http://dx.doi.org/10.1016/0378-3839(92)90015-M).
- Grain, D.A., Bolten, A.B., Bjørndal, K.A., 1995. Effects of beach nourishment on sea turtles: Review and research initiatives. *Restoration Ecol.* 3 (2), 95–104. <http://dx.doi.org/10.1111/j.1526-100X.1995.tb00082.x>.
- Guard, P., McPherson, K., Mohaupt, J., 2008. A field investigation into the groundwater dynamics of Raine Island. The University of Queensland, <http://dx.doi.org/10.14264/131499>.
- Haberer, C.M., Cirkpa, O.A., Rolle, M., Grathwohl, P., 2014. Experimental sensitivity analysis of oxygen transfer in the capillary fringe. *Groundwater* 52 (1), 37–49. <http://dx.doi.org/10.1111/gwat.12028>.
- Hannides, A., Elko, N., Humiston, K., 2019. The state of understanding of the effects of beach nourishment activities on coastal biogeochemical processes and conditions. *Shore Beach* 46–57. <http://dx.doi.org/10.34237/1008734>.
- Hegge, B.J., Masselink, G., 1991. Groundwater-table responses to wave run-up: An experimental study from western Australia. *J. Coast. Res.* 7 (3), 623–634, URL <https://www.jstor.org/stable/4297881>.
- Henderson, S.M., Bowen, A.J., 2002. Observations of surf beat forcing and dissipation. *J. Geophys. Res.: Ocean.* 107 (C11), <http://dx.doi.org/10.1029/2000JC000498>.
- Hofland, B., Chen, X., Altomare, C., Oosterlo, P., 2017. Prediction formula for the spectral wave period $T_{m-1,0}$ on mildly sloping shallow foreshores. *Coast. Eng.* 123, 21–28. <http://dx.doi.org/10.1016/j.coastaleng.2017.02.005>.
- Holding, S., Allen, D.M., Foster, S., Hsieh, A., Larocque, I., Klassen, J., Van Pelt, S.C., 2016. Groundwater vulnerability on small islands. *Nat. Clim. Chang.* 6 (12), 1100–1103. <http://dx.doi.org/10.1038/nclimate3128>.
- Holthuijsen, L.H., 2007. Waves in oceanic and coastal waters. Waves in Oceanic and Coastal Waters. Cambridge University Press, Cambridge, <http://dx.doi.org/10.1017/CBO9780511618536>.
- Horn, D.P., 2006. Measurements and modelling of beach groundwater flow in the swash-zone: a review. *Cont. Shelf Res.* 26 (5), 622–652. <http://dx.doi.org/10.1016/j.csr.2006.02.001>.
- Horrocks, J.A., Scott, N.M., 1991. Nest site location and nest success in the hawksbill turtle *Eretmochelys imbricata* in Barbados, West Indies. *Mar. Ecol. Prog. Ser.* 69, 1–8, URL <https://www.jstor.org/stable/44634759>.
- Housego, R., Raubenheimer, B., Elgar, S., Cross, S., Legner, C., Ryan, D., 2021. Coastal flooding generated by ocean wave- and surge-driven groundwater fluctuations on a sandy barrier island. *J. Hydrol.* 603, 126920. <http://dx.doi.org/10.1016/j.jhydrol.2021.126920>.
- Huff, T., Feagin, R., Figlus, J., 2020. Enhanced tide model: Improving tidal predictions with integration of wind data. *Shore Beach* 88 (2), 40–45. <http://dx.doi.org/10.34237/1008824>.
- Iribarren, C.R., Nogales, C., 1949. Protection des ports. In: *Proceedings XVIIth International Navigation Congress, Section II, Communication, Vol. 4*. Lisbon, pp. 31–80.
- Jeyaseelan, A., Balaji, R., 2015. Spectral analysis of wave elevation time histories using multi-taper method. *Ocean Eng.* 105, 242–246. <http://dx.doi.org/10.1016/j.oceaneng.2015.06.051>.
- Jost, D., Winter, J., Gallert, C., 2011. Water and Oxygen dependence of *Pseudomonas putida* growing in Silica Sand Capillary Fringes. *Vadose Zone J.* 10 (2), 532–540. <http://dx.doi.org/10.2136/vzj2010.0092>.
- Kikukawa, A., Kamezaki, N., Ota, H., 1999. Factors affecting nesting beach selection by loggerhead turtles (*Caretta caretta*): a multiple regression approach. *J. Zool.* 249 (4), 447–454. <http://dx.doi.org/10.1111/j.1469-7998.1999.tb01214.x>.
- Kreitler, C.W., Guevera, E., Granata, G., Mckalips, D., 1977. Hydrogeology of Gulf Coast aquifers, Houston-Galveston, Texas. *Gulf Coast Assoc. Geol. Soc. Trans.* 27, 72–89.
- Li, L., Cartwright, N., Nielsen, P., Lockington, D., 2004. Response of coastal groundwater table to offshore storms. *China Ocean Eng.* 18 (3), 423–431.
- Limpus, C.J., Miller, J.D., Pfaller, J.B., 2021. Flooding-induced mortality of loggerhead sea turtle eggs. *Wildl. Res.* 48 (2), 142. <http://dx.doi.org/10.1071/WR20080>.
- Lyons, M.P., von Holle, B., Weishampel, J.F., 2022. Why do sea turtle nests fail? Modeling clutch loss across the southeastern United States. *Ecosphere* 13 (3), e3988. <http://dx.doi.org/10.1002/ecs2.3988>.
- Maglio, C., Das, H., Fenner, F., 2020. Modal grain size evolution as it relates to the dredging and placement process - Galveston Island, Texas. *Coast. Eng. Proc.* (36v), 7. <http://dx.doi.org/10.9753/icce.v36v.papers.7>.
- Marquez, M., 1994. Synopsis of Biological Data on the Kemp's Ridley Turtle, *Lepidochelys kempi* (Garman, 1880). Technical Report, NOAA, Silver Spring, MD, URL https://repository.library.noaa.gov/view/noaa/6184/noaa_6184_DS1.pdf.
- Marquez, R., Carrasco, M.A., Jimenez, M.C., Peñaflores, C., Bravo, R., 2005. Kemp's and Olive Ridley Sea turtles populations status. In: Coyne, M.S., Clark, R.D. (Eds.), *Proceedings of the Twenty-First Annual Symposium on Sea Turtle Biology and Conservation*. NOAA Technical Memorandum NMFS-SEFSC-528. Philadelphia, pp. 237–239.
- Masselink, G., Turner, I.L., Williams, J., 2009. Large-scale laboratory investigation into the effect of the beach groundwater table on Gravel Beach Morphology. *J. Coast. Res.* (56), 93–97, URL <https://www.jstor.org/stable/25737544>.
- Masterson, J.P., Fienen, M.N., Thieler, E.R., Gesch, D.B., Gutierrez, B.T., Plant, N.G., 2014. Effects of sea-level rise on barrier island groundwater system dynamics – ecohydrological implications. *Ecology* 7 (3), 1064–1071. <http://dx.doi.org/10.1002/eco.1442>.
- Maurer, A.S., Johnson, M.W., 2017. Loggerhead nesting in the northern Gulf of Mexico: Importance of beach slope to nest site selection in the Mississippi Barrier Islands. *Chelonian Conserv. Biol.* 16 (2), 250–254. <http://dx.doi.org/10.2744/CCB-1256.1>.
- McGehee, A.M., 1990. Effects of moisture on eggs and hatchlings of loggerhead sea turtles (*Caretta caretta*). *Herpetologica* 46 (3), 251–258, URL <https://www.jstor.org/stable/3892967>.
- Meylan, A., 1988. Spongivory in hawksbill turtles: A diet of glass. *Science* 239 (4838), 393–395. <http://dx.doi.org/10.1126/science.239.4838.393>.
- Michael, H.A., Russoniello, C.J., Byron, L.A., 2013. Global assessment of vulnerability to sea-level rise in topography-limited and recharge-limited coastal groundwater systems. *Water Resour. Res.* 49 (4), 2228–2240. <http://dx.doi.org/10.1002/wrcr.20213>.
- Miller, J.D., Limpus, C.J., Godfrey, M., 2003. Chapter 8: Nest site selection, oviposition, eggs, development, hatching, and emergence of loggerhead turtles. In: Bolten, A.B., Witherington, B.E. (Eds.), *Loggerhead Sea Turtles*. Smithsonian Press, Washington, DC, pp. 125–143.
- Montague, C.L., 1993. Ecological engineering of inlets in southeastern florida: Design criteria for sea turtle nesting beaches. *J. Coast. Res.* 18, 267–276, URL <https://www.jstor.org/stable/25735685>.
- Mortimer, J.A., 1990. The influence of beach sand characteristics on the nesting behavior and clutch survival of Green Turtles (*Chelonia mydas*). *Copeia* 1990 (3), 802. <http://dx.doi.org/10.2307/1446446>.
- NCEI, 2023. U.S. climate normals v1.0.1. URL <https://www.ncei.noaa.gov/products/land-based-station/us-climate-normals>.
- Nel, R., Campbell, E.E., Harris, L., Hauser, L., Schoeman, D.S., McLachlan, A., du Preez, D.R., Bezuidenhout, K., Schlacher, T.A., 2014. The status of sandy beach science: Past trends, progress, and possible futures. *Estuar. Coast. Shelf Sci.* 150 (PA), 1–10. <http://dx.doi.org/10.1016/j.ecss.2014.07.016>.
- Nielsen, P., 1989. Measurements of wave setup and the coastal water table. In: *Ninth Australasian Conference on Coastal and Ocean Engineering, 1989: Preprints of Papers*. Institution of Engineers, Australia, pp. 276–280, URL <https://search.informit.org/doi/10.3316/informit.919586751063314>.
- Nielsen, P., 1990. Tidal dynamics of the water table in beaches. *Water Resour. Res.* 26 (9), 2127–2134. <http://dx.doi.org/10.1029/WR026i09p02127>.
- Nielsen, P., 1999. Groundwater dynamics and salinity in coastal barriers. *J. Coast. Res.* 15 (3), 732–740, URL <https://www.jstor.org/stable/4298987>.
- Nitime, 2019. Nitime: time-series analysis for neuroscience, v0.9. URL <https://nipy.org/nitime/documentation.html>.
- NOAA, 2024. National oceanic and atmospheric administration (NOAA) tides and currents. URL <https://tidesandcurrents.noaa.gov>.
- NWS, 2024. Galveston, scholes field. URL <https://www.weather.gov/wrh/timeseries?site=KGLS>.
- Paine, J.G., Caudle, T., Andrews, J.R., 2021. Shoreline Movement and Beach and Dune Volumetrics along the Texas Gulf Coast, 1930s to 2019. Technical Report, Bureau of Economic Geology, Austin, TX, URL https://coastal.beg.utexas.edu/shorelinechange2019/assets/glo_gsu_2019_r02_d4.pdf.
- Patino-Martinez, J., Marco, A., Quiñones, L., Hawkes, L.A., 2014. The potential future influence of sea level rise on leatherback turtle nests. *J. Exp. Mar. Biol. Ecol.* 461, 116–123. <http://dx.doi.org/10.1016/j.jembe.2014.07.021>.
- Patrício, A.R., Hawkes, L.A., Monsinjon, J.R., Godley, B.J., Fuentes, M.M.P.B., 2021. Climate change and marine turtles: recent advances and future directions. *Endanger. Species Res.* 44, 363–395. <http://dx.doi.org/10.3354/esr01110>.
- Percival, D.B., Walden, A.T., 1993. Multitaper spectral estimation. In: *Spectral Analysis for Physical Applications*. Cambridge University Press, pp. 331–377. <http://dx.doi.org/10.1017/CBO9780511622762.010>.
- Pettit, B.M., Winslow, A.G., 1957. Geology and Ground-Water Resources of Galveston County, Texas. Technical Report, USGS Water Supply Paper 1416, p. 157. <http://dx.doi.org/10.3133/wsp1416>.
- Pike, D.A., Roznik, E.A., Bell, I., 2015. Nest inundation from sea-level rise threatens sea turtle population viability. *R. Soc. Open Sci.* 2 (7), 150127. <http://dx.doi.org/10.1098/rsos.150127>.

- Pintus, K.J., Godley, B.J., McGowan, A., Broderick, A.C., 2009. Impact of clutch relocation on green turtle offspring. *J. Wildl. Manag.* 73 (7), 1151–1157. <http://dx.doi.org/10.2193/2008-103>.
- Raubenheimer, B., Guza, R.T., Elgar, S., 1999. Tidal water table fluctuations in a sandy ocean beach. *Water Resour. Res.* 35 (8), 2313–2320. <http://dx.doi.org/10.1029/1999WR900105>.
- Richardson, C.M., Davis, K.L., Ruiz-González, C., Guimond, J.A., Michael, H.A., Paldor, A., Moosdorf, N., Paytan, A., 2024. The impacts of climate change on coastal groundwater. *Nat. Rev. Earth Environ.* 5 (2), 100–119. <http://dx.doi.org/10.1038/s43017-023-00500-2>.
- Rotzoll, K., Fletcher, C.H., 2013. Assessment of groundwater inundation as a consequence of sea-level rise. *Nat. Clim. Chang.* 3 (5), 477–481. <http://dx.doi.org/10.1038/nclimate1725>.
- Seney, E., Landry, A., 2008. Movements of kemp's ridley sea turtles nesting on the upper Texas coast: implications for management. *Endanger. Species Res.* 4 (1–2), 73–84. <http://dx.doi.org/10.3354/esr00077>.
- Shaver, D.J., Caillouet, Jr., C.W., 2015. Reintroduction of Kemp's ridley (*Lepidochelys kempii*) sea turtle to Padre Island National Shoreline, Texas and its connection to head-starting. *Herpetol. Conserv. Biol.* 10 (1), 378–435, URL https://www.herpconbio.org/Volume_10/Symposium/Caillouet_etal_2015.pdf.
- Slepian, D., 1978. Prolate spheroidal wave functions, Fourier analysis, and uncertainty-V: The discrete case. *Bell Syst. Tech. J.* 57 (5), 1371–1430. <http://dx.doi.org/10.1002/j.1538-7305.1978.tb02104.x>.
- Smithers, S.G., Dawson, J.L., 2023. Beach reprofiling to improve reproductive output at the world's largest remaining green turtle rookery: Raine Island, northern Great Barrier Reef. *Ocean & Coastal Management* 231, 106385. <http://dx.doi.org/10.1016/j.ocecoaman.2022.106385>.
- Sous, D., Lambert, A., Rey, V., Michallet, H., 2013. Swash-groundwater dynamics in a sandy beach laboratory experiment. *Coast. Eng.* 80, 122–136. <http://dx.doi.org/10.1016/j.coastaleng.2013.05.006>.
- Steinitz, M.J., Salmon, M., Wyneken, J., 1998. Beach renourishment and loggerhead turtle reproduction: A seven year study at Jupiter Island. *J. Coast. Res.* 14 (3), 1000–1013, URL <http://www.jstor.org/stable/4298852>.
- Stockdon, H.F., Holman, R.A., Howd, P.A., Sallenger, A.H., 2006. Empirical parameterization of setup, swash, and runup. *Coast. Eng.* 53 (7), 573–588. <http://dx.doi.org/10.1016/j.coastaleng.2005.12.005>.
- Thomson, D., 1982. Spectrum estimation and harmonic analysis. *Proc. IEEE* 70 (9), 1055–1096. <http://dx.doi.org/10.1109/PROC.1982.12433>.
- Thomson, D., 2007. Jackknifing multitaper spectrum estimates. *IEEE Signal Process. Mag.* 24 (4), 20–30. <http://dx.doi.org/10.1109/MSP.2007.4286561>.
- Thomson, J., Elgar, S., Raubenheimer, B., Herbers, T.H.C., Guza, R.T., 2006. Tidal modulation of infragravity waves via nonlinear energy losses in the surfzone. *Geophys. Res. Lett.* 33 (5), <http://dx.doi.org/10.1029/2005GL025514>.
- Turner, I.L., 1993. The total water content of sandy beaches. *J. Coast. Res.* (15), 11–26, URL <https://www.jstor.org/stable/25735720>.
- Turner, I.L., Coates, B.P., Acworth, R.I., 1997. Tides, waves and the super-elevation of groundwater at the coast. *J. Coast. Res.* 13 (1), 46–60, URL <http://www.jstor.org/stable/4298589>.
- Turner, I.L., Nielsen, P., 1997. Rapid water table fluctuations within the beach face: Implications for swash zone sediment mobility? *Coast. Eng.* 32 (1), 45–59. [http://dx.doi.org/10.1016/S0378-3839\(97\)00015-X](http://dx.doi.org/10.1016/S0378-3839(97)00015-X).
- USACE, 2021. Coastal Texas Protection and Restoration Feasibility Study. Final Report. Technical Report, U.S. Army Corps of Engineers. Galveston District and Texas General Land Office, p. 192, URL https://www.swg.usace.army.mil/Portals/26/Coastal%20TX%20Protection%20and%20Restoration%20FINAL%20Feasibility%20Report_20210827.pdf.
- USACE, 2022. Galveston 204 CAP – Beach Nourishment, Engineering Appendix, Hydrology and Hydraulics. Technical Report, US Army Corps of Engineers, Galveston District, Galveston, TX, URL https://www.swg.usace.army.mil/Portals/26/HHGalv204AppxA5may22%20-%20DRAFT_1.pdf.
- Valverde, R.A., Holzwart, K.R., 2017. Sea turtles of the Gulf of Mexico. In: Ward, C.H. (Ed.), *Habitats and Biota of the Gulf of Mexico: Before the Deepwater Horizon Oil Spill*. Springer New York, New York, NY, pp. 1189–1351. http://dx.doi.org/10.1007/978-1-4939-3456-0_3.
- van der Grinten, M.J., Christiaanse, J.C., Reniers, A.J., Taal, F., Figlus, J., Antolínez, J.A., 2025. Wave runup extraction on dissipative beaches: New video-based methods. *Coast. Eng.* 104757. <http://dx.doi.org/10.1016/j.coastaleng.2025.104757>.
- Van Hoek, M., Jia, L., Zhou, J., Zheng, C., Menenti, M., 2016. Early drought detection by spectral analysis of satellite time series of precipitation and normalized difference vegetation index (NDVI). *Remote. Sens.* 8 (5), 422. <http://dx.doi.org/10.3390/rs8050422>.
- Van Houtan, K.S., Bass, O.L., 2007. Stormy oceans are associated with declines in sea turtle hatching. *Curr. Biol.* 17 (15), R590–R591. <http://dx.doi.org/10.1016/j.cub.2007.06.021>.
- Ware, M., Ceriani, S., Long, J., Fuentes, M.M.P.B., 2021. Exposure of loggerhead sea Turtle Nests to waves in the Florida Panhandle. *Remote. Sens.* 13 (14), 2654. <http://dx.doi.org/10.3390/rs13142654>.
- Ware, M., Fuentes, M.M., 2018. A comparison of methods used to monitor groundwater inundation of sea turtle nests. *J. Exp. Mar. Biol. Ecol.* 503, 1–7. <http://dx.doi.org/10.1016/j.jembe.2018.02.001>.
- Welch, P., 1967. The use of fast Fourier transform for the estimation of power spectra: A method based on time averaging over short, modified periodograms. *IEEE Trans. Audio Electroacoust.* 15 (2), 70–73. <http://dx.doi.org/10.1109/TAU.1967.1161901>.
- Yamamoto, K.H., Powell, R.L., Anderson, S., Sutton, P.C., 2012. Using LiDAR to quantify topographic and bathymetric details for sea turtle nesting beaches in florida. *Remote Sens. Environ.* 125, 125–133. <http://dx.doi.org/10.1016/j.rse.2012.07.016>.
- Zheng, F., Westra, S., Sisson, S.A., 2013. Quantifying the dependence between extreme rainfall and storm surge in the coastal zone. *J. Hydrol.* 505, 172–187. <http://dx.doi.org/10.1016/j.jhydrol.2013.09.054>.